

Lethal surface ozone concentrations are possible on habitable zone exoplanets

G. J. COOKE ^{1,2,*} D. R. MARSH ² C. WALSH ² AND F. SAINSBURY-MARTINEZ ²

¹*Institute of Astronomy, University of Cambridge, UK.*

²*School of Physics and Astronomy, University of Leeds, Leeds, LS2 9JT, UK*

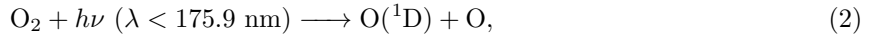
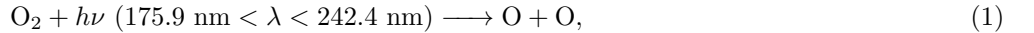
ABSTRACT

Ozone (O₃) is important for the survival of life on Earth because it shields the surface from ionising ultraviolet (UV) radiation. However, the existence of O₃ in Earth's atmosphere is not always beneficial. Resulting from anthropogenic activity, O₃ exists as a biologically harmful pollutant at the surface when it forms in the presence of sunlight and other pollutants. As a strong oxidiser, O₃ can be lethal to several different organisms; thus, when assessing the potential habitability of an exoplanet, a key part is determining whether toxic gases could be present at its surface. Using the Whole Atmosphere Community Climate Model version 6 (WACCM6; a three-dimensional chemistry-climate model), twelve atmospheric simulations of the terrestrial exoplanet TRAPPIST-1 e are performed with a variety of O₂ concentrations and assuming two different stellar spectra proposed in the literature. Four atmospheric simulations of the exoplanet Proxima Centauri b are also included. Some scenarios for both exoplanets exhibit time-averaged surface O₃ mixing ratios exceeding harmful levels of 40 ppbv, with 2200 ppbv the maximum concentration found in the cases simulated. These concentrations are toxic and can be fatal to most life on Earth. In other scenarios O₃ remains under harmful limits over a significant fraction of the surface, despite there being present regions which may prove inhospitable. In the case that O₃ is detected in a terrestrial exoplanet's atmosphere, determining the surface concentration is an important step when evaluating a planet's habitability.

Keywords: Exoplanets (498) — Exoplanet atmospheres (487) — Habitable planets (695) — Exoplanet atmospheric composition (2021)

1. INTRODUCTION

Molecular oxygen (O₂) makes up 21% by volume of Earth's atmospheric composition and is required for aerobic respiration, provides a fuel for combustion, and gives rise to the 'ozone layer'. In an atmosphere with O₂ and sufficient ultraviolet (UV) irradiation at wavelengths shortward of 242.4 nm, O₂ is photodissociated into atomic oxygen (O):



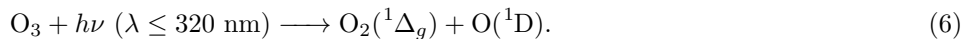
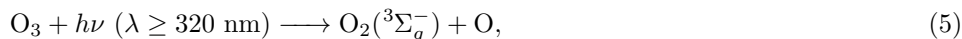
where $h\nu$ represents a photon of frequency ν , and h is Planck's constant¹. O₂ and O can form ozone (O₃) via the following 3 body reaction:



where M is any third body (usually N₂ or O₂ on Earth due to their relatively high abundance). O₃ can also be destroyed through photolysis, or by reacting with atomic oxygen:

* E-mail: gjc53@cam.ac.uk

¹ O(¹D) is the first excited state of atomic oxygen, where 1 represents the spin multiplicity and D is the spectroscopic notation for total orbital angular momentum. Note that the ground state of atomic oxygen can be written as O(³P)



On modern-day Earth, the majority of O_3 resides in the stratosphere, roughly 15 to 35 km above the surface in the ‘ozone layer’ (Brasseur & Solomon 2005). Here, O_3 is beneficial for surface-dwelling life, absorbing biologically harmful UV radiation and providing a partial screen for life exposed to the Sun’s radiation. Even though the majority of Earth’s O_3 is produced in the equatorial stratosphere, there exists a larger column of O_3 at higher latitudes. This is because O_3 is distributed through a seasonal equator-to-pole circulation driven by atmospheric gravity waves, known as the Brewer-Dobson circulation (Butchart 2014). The Brewer-Dobson circulation has been observed to accelerate and decelerate due to climate change (Garcia & Randel 2008; Butchart 2014; Fu et al. 2019), consequently affecting regional composition and temperatures near the tropopause and lower stratosphere.

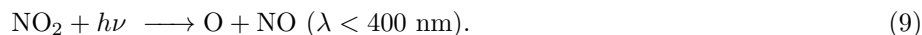
The situation in the troposphere (the lowest atmospheric layer where temperature decreases with altitude) is rather different, because the photolysis rate of O_2 is significantly lower here than in the stratosphere. Near the surface, volatile organic compounds (VOCs) can also contribute to O_3 formation. Hydrocarbon emissions emanate from plants (e.g., isoprene, α -pinene; Chameides et al. 1988; Sharkey et al. 2008) and, on modern day Earth, from anthropogenic activity (e.g., naphthalene, acetone, formaldehyde, and many others; Atkinson 2000). When photooxidation of hydrocarbons occurs in presence of nitrogen oxides, O_3 can eventually be produced through the ‘smog mechanism’ (Haagen-Smit 1952). For example, NO_2 can be produced when OH reacts with a hydrocarbon (Sillman 1999), RH (R is an organic group), producing RO_2 and H_2O :



RO_2 leads to NO_2 formation via



Then, NO_2 is photolysed in the presence of UV light:



The O produced can lead to reaction 3, making O_3 at low altitudes. On Earth, surface O_3 is low at night when it is removed through reaction with NO,



and O_3 increases during the day due to photochemistry (Sillman 1999). Reaction 10 is part of a catalytic cycle, where a catalyst (X) leads to the destruction of O_3 , but is ultimately not used up in the overall reaction, such that



At the surface, O_3 is considered a pollutant because it causes oxidative stress to plants, insects, and animals, including humans (Avnery et al. 2011; Silva et al. 2013; Valavanidis et al. 2013; Squire et al. 2014; Démares et al. 2022). Oxidative stress is a chemical imbalance between oxidants and reductants inside an organism that can lead to molecular and biological damage (Lykkesfeldt & Svendsen 2007; Sies et al. 2017). It has been demonstrated in many scenarios that O_3 is an antimicrobial agent, capable of microbial inactivation of fungi, viruses, and bacteria (Kim et al.

1999; Guzel-Seydim et al. 2004; Najafi & Khodaparast 2009; Fontes et al. 2012; Epelle et al. 2023; Rojas-Valencia 2011). For instance, the removal of microbiota was demonstrated using ozonation of the air (Epelle et al. 2022), and aqueous O_3 is effective at inactivating microorganisms (Premjit et al. 2022). Additionally, O_3 has been found to be toxic across a wide range of organisms, including guinea pigs, rats, mice (Giese & Christensen 1954; Stokinger 1965), terrestrial plants (Rich 1964; Bytnerowicz et al. 1993; Sandermann Jr 1996; Rao & Davis 2001; Ramya et al. 2023), aquatic life (Jones et al. 2006), protozoa (Erickson & Ortega 2006), and algae (Hu et al. 2003; Gonçalves & Gagnon 2011).

It is useful to consider some quantities to illustrate ozone’s danger to life. For example, 40 parts per billion by volume (ppbv) of O_3 is defined by the World Health Organisation (WHO) as a critical limit above which crop yield and species biomass may be reduced (World Health Organization et al. 2000). The WHO stated that significant health effects were exhibited by humans at 80 ppbv (World Health Organization et al. 2000), with O_3 damaging lung function at 100 ppbv for 1 – 8 hours of exposure. Indeed, years of evidence has indicated that long-term exposure to O_3 appears to be related to premature human deaths (Bell et al. 2006; Turner et al. 2016; Sun et al. 2022). For instance, O_3 was attributed to 6,000 premature deaths in the EU in 2013 (Nuvolone et al. 2018), and a modelling study by Malashock et al. (2022) calculated global O_3 -attributable mortality in 2019 was 423,100 deaths (95% confidence interval of 223,200 – 659,400). The majority (77%) of these were estimated to have occurred in Asia, where ground level O_3 concentrations were relatively high (Malashock et al. 2022). Furthermore, Feng et al. (2022) estimated that in East Asia, the reduced crop yield to O_3 pollution costs US\$63 billion annually. If O_3 is detrimental to life on Earth, then the same could be possible for extraterrestrial life. Due to ozone’s powerful oxidising capacity (Menzel 1984; Iriti & Faoro 2007), it is possible that its toxicity to life could be ubiquitous. It is highly reactive, ranking amongst the highest oxidisers². O_3 , when internal to an organism, causes oxidative stress by releasing reactive oxygen species, which can then cause damage to proteins, DNA, and ultimately result in genetic mutations and cell growth that potentially turns into cancer (Klaunig et al. 2010).

O_3 , its spatial distribution on Earth, and its impact on terrestrial organisms, has been well studied. Less explored have been the implications of O_3 in exoplanet atmospheres. Hundreds of terrestrial exoplanets, rocky planets orbiting stars other than the Sun, have been detected in our galaxy. Many of these are in the purported habitable zone (HZ) around their host star (the region in which liquid water could persist on the surface of a rocky exoplanet; Kasting et al. 1993), although the potential for exoplanets and exomoons to be habitable goes beyond the traditional terrestrial-like HZ (see e.g., Colose et al. 2019; Tjoa et al. 2020; Madhusudhan et al. 2021). If extraterrestrial life exists, then at some point in its evolution, it is possible that O_2 could be biologically produced just as it is on Earth, although there are several situations where O_2 could be abiotically produced in high quantities (Des Marais et al. 2002; Wordsworth & Pierrehumbert 2014; Domagal-Goldman et al. 2014; Luger & Barnes 2015; Kleinböhl et al. 2018). These scenarios include major water loss from photolysis (Wordsworth & Pierrehumbert 2014; Luger & Barnes 2015) and high rates of CO_2 photodissociation (Gao et al. 2015; Harman et al. 2015; Schwieterman et al. 2016). Either way, O_3 is a molecule of interest because its detection can indicate the presence of atmospheric O_2 (Leger et al. 1993; Kozakis et al. 2022). Additionally, O_3 has strong spectroscopic signatures in both direct imaging and transmission spectra observations at relatively small volume mixing ratios (e.g., between 10^{-7} and 10^{-5} ; Reinhard et al. 2017; Schwieterman et al. 2018; Kozakis et al. 2022). Due to this property, some work has shown that in particular scenarios, O_3 may be easier to detect than O_2 (Reinhard et al. 2017; Kozakis et al. 2022; Cooke et al. 2023). To date, O_3 has not yet been detected in the atmosphere of a terrestrial exoplanet, so the only estimates of the full O_3 spatial distribution on exoplanets arises from three-dimensional chemistry-climate simulations.

Tidally locked exoplanets are exoplanets that have a rotational period equal to their orbital period (P), such that they rotate synchronously (Joshi et al. 1997; Showman & Polvani 2011; Pierrehumbert & Hammond 2019). Carone et al. (2018) simulated tidally locked terrestrial exoplanets with orbital periods of 1 – 100 days, finding that their atmospheric circulation depends in part on rotation rate. For $P < 25$ days, it was established that stratospheric transport could occur from the pole to the equator (described as an ‘Anti-Brewer Dosbon circulation’), or vice versa, depending on stratospheric wind breaking and the location of the planetary-scale Rossby waves (e.g., tropical or extratropical). At rotational periods greater than 25 days, the results from Carone et al. (2018) showed that a thermally driven circulation between the dayside and nightside could widely distribute air parcels. Yates et al. (2020)

² F_2 is the strongest oxidiser with a standard electrode potential of 2.87 eV, whilst O_3 usually ranks second and has a standard electrode potential of 2.075 eV (Kishimoto & Arai 2022). The standard electrode potential is “The value of the standard emf of a cell in which molecular hydrogen under standard pressure is oxidized to solvated protons at the left-hand electrode.” (McNaught et al. 1997)

used the Unified Model (UM) to simulate Proxima Centauri b (assuming a terrestrial exoplanet with a 11.18 day rotation period) in a slab ocean aquaplanet configuration, and found that the nightside O_3 lifetime is much higher than it is on the dayside. The same conclusion was reached by [Proedrou & Hocke \(2016\)](#), who simulated a tidally locked Earth with a rotational period of 365 days (no Brewer-Dobson circulation was present on this simulated exoplanet). [Chen et al. \(2019\)](#) used WACCM4, and reported that the pole-to-equator transport predicted by [Carone et al. \(2018\)](#) was present in two of their chemistry-climate simulations for terrestrial exoplanets with periods of 4.11 days and 7.91 days, and total irradiation of $1.0 S_0$ and $1.1 S_0$, respectively. Recently, [Braam et al. \(2023\)](#) used the UM and found that O_3 is produced on the dayside and transported to the nightside, with downwelling motions causing O_3 to move into the troposphere at the positions of the nightside gyres. The use of a slab ocean aquaplanet configuration results in highly symmetric winds and chemical transport.

Only a few studies have commented upon surface O_3 in paleo atmospheres and exoplanet atmospheres. [Grenfell et al. \(2013\)](#) used a one-dimensional radiative-convective-photochemical model to investigate the atmospheric properties of super Earths around M0 to M7 stars and with surface gravity of $1 g$ and $3 g$ (where $g = 9.81 \text{ m s}^{-2}$). Whilst the smog mechanism was important for O_3 production around later spectral types, the surface O_3 concentrations did not exceed harmful levels. [Grenfell et al. \(2006\)](#) used a box model and showed how the smog mechanism could produce ground-level O_3 up to 3500 ppbv during the Proterozoic (2.4 – 0.541 Gyr ago) on Earth at 1% the present atmospheric level (PAL) of O_2 . During the Proterozoic, O_2 concentrations could have ranged between 10^{-5} – 1 times the PAL of O_2 ([Large et al. 2019](#); [Catling & Zahnle 2020](#); [Steadman et al. 2020](#); [Lyons et al. 2021](#)).

The study by [Grenfell et al. \(2006\)](#) is the only example of a simulated atmosphere which differs to modern Earth where harmful levels of O_3 have been discussed, although the narrative focused on how O_3 would have shielded the early Earth from UV radiation. No previous work has discussed the hypothetical dangers from O_3 for extraterrestrial life on exoplanets and also used a 3D chemistry-climate model which accounts for horizontal transport. This work presents simulations of the exoplanets TRAPPIST-1 e and Proxima Centauri b using WACCM6, a 3D chemistry-climate model. Both exoplanets are located in the supposed HZ of their host stars, and TRAPPIST-1 e is a target for JWST transmission spectra observations. Proxima Centauri b orbits the star Proxima Centauri (M5.5V spectral type, with a stellar effective temperature of 2,992 K; [Pineda et al. 2021](#)), which is the closest star to the Sun (1.3 pc; [Gaia Collaboration et al. 2016](#)), making it an exciting target for future observations ([Fowler et al. 2023](#)). TRAPPIST-1 e is a roughly Earth-sized exoplanet orbiting in the HZ around its ultra cool M8V (stellar effective temperature of 2,566 K; [Agol et al. 2021](#)) dwarf host star, TRAPPIST-1. Whilst faint, TRAPPIST-1 is relatively close at a distance of 12.4 pc (40.5 light years). As host of 6 other terrestrial exoplanets, the TRAPPIST-1 system is a prime target to test theories of planetary system formation and evolution, by confirming whether atmospheres exist on any of the exoplanets, and characterising their properties if they do. To date, analysis of observations of the exoplanetary thermal emission with JWST suggests that the two innermost exoplanets, TRAPPIST-1b and c, have either thin atmospheres, or no atmosphere at all ([Zieba et al. 2023](#); [Greene et al. 2023](#)). Assuming that Earth-like atmospheres exist on both TRAPPIST-1 e and Proxima Centauri b, we investigate the abundance and distribution of O_3 concentrations in different simulated scenarios, and discuss the implications for the habitability of oxygenated worlds.

2. SIMULATIONS

We use the three-dimensional Earth System Model WACCM6 ([Gettelman et al. 2019](#)) to perform twelve simulations of possible climates of TRAPPIST-1 e, and four possible climate simulations of Proxima Centauri b. WACCM6 is a configuration of the Coupled Earth System Model (CESM), and we use version 2.1.3 (CESM2.1.3). In each simulation the initial conditions represent the approximate conditions of Earth’s pre-industrial (PI) atmosphere for the year 1850. The simulations have the modern ocean and land configuration, a horizontal resolution of 1.875° by 2.5° (96 latitude points and 144 longitude points), and 70 vertical atmospheric levels from 1000 hPa to 4.5×10^{-6} hPa. Both the atmosphere and ocean models are set up to be fully interactive so that they respond to physical changes such as temperature. Because it is likely that Proxima Centauri b and TRAPPIST-1 e rotate synchronously (they may be tidally locked to their host star, although spin-orbit resonance states are plausible; [Ribas et al. 2016](#); [Renaud et al. 2021](#)), the substellar point is fixed. This is done by fixing the solar zenith angle in each grid cell. The exoplanet’s obliquity and orbital eccentricity are set to zero. We run WACCM6 with middle atmosphere chemistry which is described in [Emmons et al. \(2020\)](#), where further details can be found. This chemical mechanism in the WACCM6 simulations has 98 chemical species and 298 chemical reactions, including both the photochemical and heterogeneous reactions that are necessary to simulate the atmospheric conditions of 1850, and crucially, O_3 chemistry. O_3 pollution

due to VOCs is not simulated. The atmospheric time step, Δt , is 30 minutes. The concentrations of 75 species are computed using the implicit method, which considers the chemical system at time t and $t + \Delta t$ to evaluate the system at the future time step $t + \Delta t$ (Sandu et al. 1997). 22 long-lived species are computed with the explicit method, which calculates the chemical system at a later time $t + \Delta t$ by considering the current system at time t (Brasseur & Solomon 2005). N_2 is invariant in each simulation, and its mixing ratio in each simulation is adapted to ensure that the atmosphere maintains a surface pressure of 1,000 hPa. Following the work by Ji et al. (2023), we include absorption by O_3 , O_2 , CO_2 and H_2O in the Schumann-Runge bands (175 – 192 nm).

‘Dry deposition’ is the process through which atmospheric trace gases and particulate matter are deposited on Earth’s surface and are removed from the atmosphere, and is an atmospheric sink of O_3 . Dry deposition in WACCM6 (Emmons et al. 2020) was updated following Val Martin et al. (2014), and was originally based on a parameterisation from Wesely (1989). The parameterisation accounts for variables such as the aerodynamic resistance and the surface resistance, and is influenced by vegetation, if present.

We assume TRAPPIST-1 e receives 900 W m^{-2} of irradiation and that Proxima Centauri b receives 884 W m^{-2} ($0.66 S_0$ and $0.65 S_0$ respectively, where S_0 is the total insolation that the Earth receives). This is consistent with previous work on Proxima Centauri b (Boutle et al. 2017; Yates et al. 2020; Braam et al. 2022; Ridgway et al. 2023) and with the TRAPPIST-1 Habitable Atmosphere Intercomparison project (THAI; Fauchez et al. 2020; Turbet et al. 2022). Proxima Centauri b was detected using the radial velocity method and has a minimum mass measured of $M_P \sin i = 1.07 M_\oplus$ (Faria et al. 2022) only, where M_P is the mass of the exoplanet and i is the inclination angle of the planetary orbit. Therefore, a recently estimated mass-radius relationship from Otegi et al. (2020), given as $R_p = 1.03 M_p^{0.29}$, was used to estimate the planetary radius. Assuming an optimistic mass of $M_P = 1.07 M_\oplus$, this

Table 1. The sixteen simulations used in this study are listed. Twelve for TRAPPIST-1 e: six with the P19 spectrum (Peacock et al. 2019) and six with the W21 spectrum (Wilson et al. 2021b). There are four simulations of Proxima Centauri b, where the MUSCLES spectrum of Proxima Centauri (see text for details) is used as stellar input. Each simulation started with the pre-industrial (PI) WACCM6 simulation composition. Each set of six TRAPPIST-1 e simulations includes three with the present atmospheric level of O_2 (0.21 by volume, all denoted as “PI”); one where the substellar point is placed over the Pacific Ocean, one where it is placed over Africa (SPL), and one where it is not tidally locked and the rotation rate is 1 Earth day (noTL). Then, the 10% PAL, 1% PAL, and 0.1% PAL simulations have reduced O_2 mixing ratios from the PI simulation by 10, 100, and 1000 times, respectively. Each of the TRAPPIST-1 e simulations receive a total instellation of 900 W m^{-2} , and the Proxima Centauri b simulations receive 884 W m^{-2} of irradiation. The Proxima Centauri b simulations include the PI, 10% PAL, 1% PAL, and 0.1% PAL cases. The simulated radius and mass of TRAPPIST-1 e are $0.91 R_\oplus$ and $0.772 M_\oplus$, respectively. For Proxima Centauri b, the radius and mass are $1.05 R_\oplus$ and $1.07 M_\oplus$, respectively. The \oplus subscript denotes values relative to the Earth. The orbital parameters assume zero eccentricity and 0° obliquity, and the table lists the period P and the longitude of the substellar point (SP) relative to Earth’s coordinates (the latitude of the SP is always 0°). Each simulation has been run out for at least 250 model Earth years.

| Simulation | Planet | Spectrum | O_2 mixing ratio [PAL] | Orbital parameters |
|--------------|--------------------|------------|--------------------------|--|
| W21 PI | TRAPPIST-1 e | W21 | 1.000 | $P = 6.1\text{d}$, SP = 180° lon |
| W21 PI noTL | TRAPPIST-1 e | W21 | 1.000 | $P = 1\text{d}$ |
| W21 PI SPL | TRAPPIST-1 e | W21 | 1.000 | $P = 6.1\text{d}$, SP = 30° lon |
| W21 10% PAL | TRAPPIST-1 e | W21 | 0.100 | $P = 6.1\text{d}$, SP = 180° lon |
| W21 1% PAL | TRAPPIST-1 e | W21 | 0.010 | $P = 6.1\text{d}$, SP = 180° lon |
| W21 0.1% PAL | TRAPPIST-1 e | W21 | 0.001 | $P = 6.1\text{d}$, SP = 180° lon |
| P19 PI | TRAPPIST-1 e | P19 | 1.000 | $P = 6.1\text{d}$, SP = 180° lon |
| P19 PI noTL | TRAPPIST-1 e | P19 | 1.000 | $P = 1\text{d}$ |
| P19 PI SPL | TRAPPIST-1 e | P19 | 1.000 | $P = 6.1\text{d}$, SP = 30° lon |
| P19 10% PAL | TRAPPIST-1 e | P19 | 0.100 | $P = 6.1\text{d}$, SP = 180° lon |
| P19 1% PAL | TRAPPIST-1 e | P19 | 0.010 | $P = 6.1\text{d}$, SP = 180° lon |
| P19 0.1% PAL | TRAPPIST-1 e | P19 | 0.001 | $P = 6.1\text{d}$, SP = 180° lon |
| PCb PI | Proxima Centauri b | PC MUSCLES | 1.000 | $P = 11.18\text{d}$, SP = 180° lon |
| PCb 10% PAL | Proxima Centauri b | PC MUSCLES | 0.100 | $P = 11.18\text{d}$, SP = 180° lon |
| PCb 1% PAL | Proxima Centauri b | PC MUSCLES | 0.010 | $P = 11.18\text{d}$, SP = 180° lon |
| PCb 0.1% PAL | Proxima Centauri b | PC MUSCLES | 0.001 | $P = 11.18\text{d}$, SP = 180° lon |

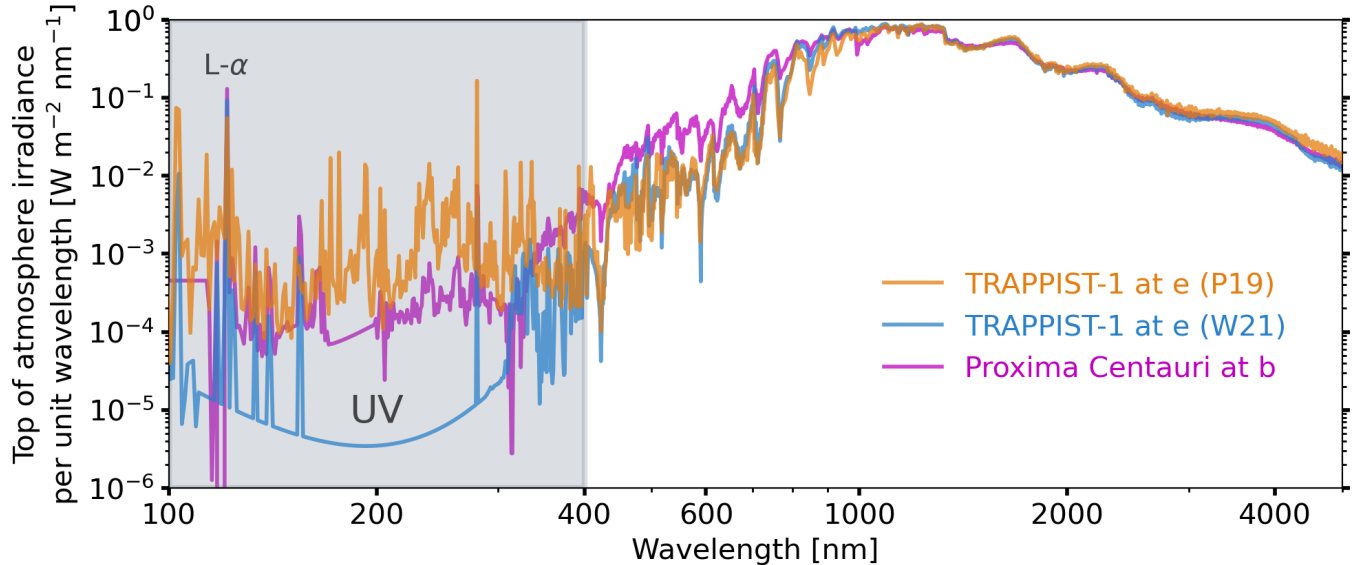


Figure 1. The three stellar input spectra used for the WACCM6 simulations are the PC MUSCLES spectrum for Proxima Centauri at b (magenta), the [Peacock et al. \(2019\)](#) (P19; orange) and [Wilson et al. \(2021b\)](#) (W21; blue) spectra for TRAPPIST-1 at e. The top of atmosphere irradiance per unit wavelength is shown against the wavelength in nm. In the simulations, TRAPPIST-1 e receives 900 W m^{-2} of irradiation ($0.66 S_{\oplus}$, where S_{\oplus} is the total insolation received by the Earth), and Proxima Centauri b receives 884 W m^{-2} ($0.65 S_{\oplus}$). The UV range is highlighted in grey between 100 – 400 nm, and the Lyman- α line is labelled. The average difference between the TRAPPIST-1 spectra in the UV range is a factor of 500, with a difference of up to 5000 in some wavelength bins.

places the radius of Proxima Centauri as $1.05 R_{\oplus}$, and the surface gravity of Proxima Centauri b at 12.2 m s^{-2} . In our simulations, TRAPPIST-1 e is set to have a mass of $0.772 M_{\oplus}$ and a radius of $0.91 R_{\oplus}$, consistent with the THAI project and transit timing variations (TTVs) from [Grimm et al. \(2018\)](#). The surface gravity of TRAPPIST-1 e is therefore set to 9.14 m s^{-2} .

Two semi-empirical stellar spectra were used in the TRAPPIST-1 e simulations. [Peacock et al. \(2019\)](#), henceforth known as P19, modelled the stellar energy distribution (SED) of TRAPPIST-1 and produced model 1A, 2A, and 2B, of which we use model 1A (version 1; [Peacock 2020](#)). More recently, [Wilson et al. \(2021b\)](#), hereafter known as W21, used further HST observations to produce a semi-empirical SED of TRAPPIST-1 (version 1; [Wilson et al. 2021a](#)) as part of the Mega-MUSCLES series ([Froning et al. 2019](#); [Wilson et al. 2021b](#)). Details of their spectra can be found in the aforementioned references. Both the stellar spectra are included here to illustrate how different strengths and shapes of the incoming UV radiation environment can affect the abundance and distribution of surface O_3 . For Proxima Centauri b, we use the GJ 551 MUSCLES (version 2.2; [France et al. 2016](#); [Youngblood et al. 2016](#); [Loyd et al. 2016](#)) spectrum as input³. GJ 551 is the Gliese–Jahreiß catalog name for Proxima Centauri.

Note that the TRAPPIST-1 e simulations were started in the year 2020, before [Agol et al. \(2021\)](#) published updates to planetary parameters in the TRAPPIST-1 system. For TRAPPIST-1 e, [Agol et al. \(2021\)](#) gave mass and radius values of $0.69 M_{\oplus}$ and $0.92 R_{\oplus}$, respectively, meaning the surface gravity would be 8.015 m s^{-2} , instead of 9.14 m s^{-2} as used here. Using these updated values, the scale height of the atmosphere would increase, but we expect that simulations with the parameters from [Agol et al. \(2021\)](#) would produce similar surface O_3 mixing ratios to the ones we present here. Only the minimum mass has been measured for Proxima Centauri b, so it is conceivable that it may have a larger mass and radius than the values used here. [Brugger et al. \(2016\)](#) estimated the radius to be in the range $0.94 - 1.40 R_{\oplus}$, placing it somewhere between a Mercury-like exoplanet and an ocean-like world. Regardless, with M-dwarf stars being so numerous, it is plausible that somewhere there exists an exoplanet with similar size and instellation, such that these simulations remain useful should Proxima Centauri b eventually be confirmed to have a mass or radius which is significantly larger.

³ GJ 551 found at <https://archive.stsci.edu/prepds/muscles/>

A summary of the simulations is given in Table 1. For TRAPPIST-1 e, six simulations use the P19 (stronger UV) spectrum, and six simulations use the W21 (weaker UV) spectrum. For both exoplanets, atmospheric concentrations of O₂ at the present atmospheric level (PI; 0.21 by volume), 10% PAL, 1% PAL, and 0.1% PAL, are simulated. For TRAPPIST-1 e, we move the substellar point for the 100% PAL simulation between the Pacific Ocean (180° longitude; PI case) and Africa (30° longitude; PI SPL case). We run two simulations which are not tidally locked and have a rotational period of 1 day. Whether a slab or dynamic ocean is implemented, and whether the land or ocean is at the substellar point, can modulate the climatology of exoplanets (Hu & Yang 2014; Lewis et al. 2018; Del Genio et al. 2019; Salazar et al. 2020; Zhao et al. 2021; Macdonald et al. 2022; Olson et al. 2022). Salazar et al. (2020) found that broad climate differences between models (ROCKE-3D and the UM) were larger than the difference between a slab ocean and a dynamic ocean. Because of this previous work, and the fact that the PI and PI SPL simulations show only small globally averaged chemical differences in O₃, and due to computational expense (WACCM6 takes 1,332 core-hours per simulated year to run), we do not simulate the substellar point over land in any of the reduced O₂ cases. Each simulation has been run out for at least 250 model Earth years, and then we present the last year of data (365 Earth days). The full details of the model set-up, alongside simulation scripts, are available via GitHub⁴.

3. RESULTS

3.1. Surface ozone concentrations

Fig. 2 shows the time-averaged distribution of O₃ at the atmospheric level closest to surface for the cases which have time-averaged surface O₃ mixing ratios of 40 ppbv or greater. We use 40 ppbv as a lower cut-off for harmful levels of surface O₃ (World Health Organization et al. 2000). Grey indicates regions below 40 ppbv, whilst the yellow-orange-purple colour map indicates regions where O₃ exceeds 40 ppbv.

The TRAPPIST-1 e (TP-1 e) P19 PI, PI SPL, no TL, and W21 0.1% PAL simulations everywhere exceed 40 ppbv for surface O₃. The P19 PI simulation has a maximum mixing ratio of 2200 ppbv, which is the largest surface mixing ratio in all of the simulations presented. In the P19 PI and 0.1% PAL simulations and the W21 0.1% PAL simulation, specific locations (e.g., Antarctica or Greenland) have extremely high mixing ratios, exceeding 1000 ppbv, which is deadly to some organisms on Earth. On the other hand, the W21 PI, PI SPL, and noTL simulations everywhere have O₃ mixing ratios below 40 ppbv, and are not shown. The low O₃ surface concentrations are a consequence of the upper atmosphere efficiently absorbing UV such that insufficient UV reaches altitudes closer to the planetary surface to synthesise enough O₃. The P19 10%, 1%, and 0.1% PAL simulations, and the W21 1%, simulation, have some areas where O₃ exceeds 40 ppbv, whilst maintaining regions below this limit. For the Proxima Centauri b (PCb) cases, the PI, 10% PAL, and 1% PAL cases have surface O₃ levels below 40 ppbv everywhere. For the 0.1% PAL PCb scenario, surface O₃ everywhere exceeds 40 ppbv and has an global mean mixing ratio of 203 ppbv.

In terms of time variability, the surface O₃ concentrations are not static. Taking the last year of simulated data and averaging each calendar month, the fraction of land for each simulation where surface O₃ concentrations are under 40 ppbv is given in Table 2. For example, the P19 10%, 1%, and 0.1% PAL simulations have monthly O₃ surface concentrations under harmful levels varying between 12 – 44%, 75 – 83%, and 4 – 9% of the total surface area. Considering all these scenarios, the prospect is raised for safe areas on exoplanets which are sheltered from hazardous O₃ concentrations found at other locations. Meanwhile, some locations will fluctuate between toxic and safe levels. Only the P19 PI noTL simulation has surface O₃ mixing ratios that everywhere exceed 40 ppbv throughout the final year of data.

The bars in Fig. 3a indicate the full range of surface O₃ mixing ratios in each of the tidally locked simulations where the substellar point is placed over ocean, with the global mean surface concentrations indicated by the points. Simulations of Earth (using WACCM6) at atmospheric O₂ mixing ratios between 0.1% – 150% PAL from data from Cooke et al. (2022) are given for comparison. Fig. 3b presents the same data for the TP-1 e PI scenarios. The TP-1 e W21 PI and 10% PAL cases have a large range in surface O₃ concentrations, spanning 7 and 8 orders of magnitude, respectively. All other TP-1 e simulations span 5 orders of magnitude or less, with the Earth simulations spanning only one order of magnitude. The PCb simulations span between 9 and 2 orders of magnitude. Whilst both the PI and PI SPL simulations with the P19 spectrum have harmful O₃ mixing ratios at the surface, the mean surface O₃ mixing ratio is reduced by 1.7 times when the substellar point is placed over land (PI SPL case). In contrast, the W21 PI SPL case has 2.0 times the mean surface O₃ mixing ratio of the W21 PI case. Additionally, the noTL cases

⁴ https://github.com/exo-cesm/CESM2.1.3/tree/main/Tidally_locked_exoplanets

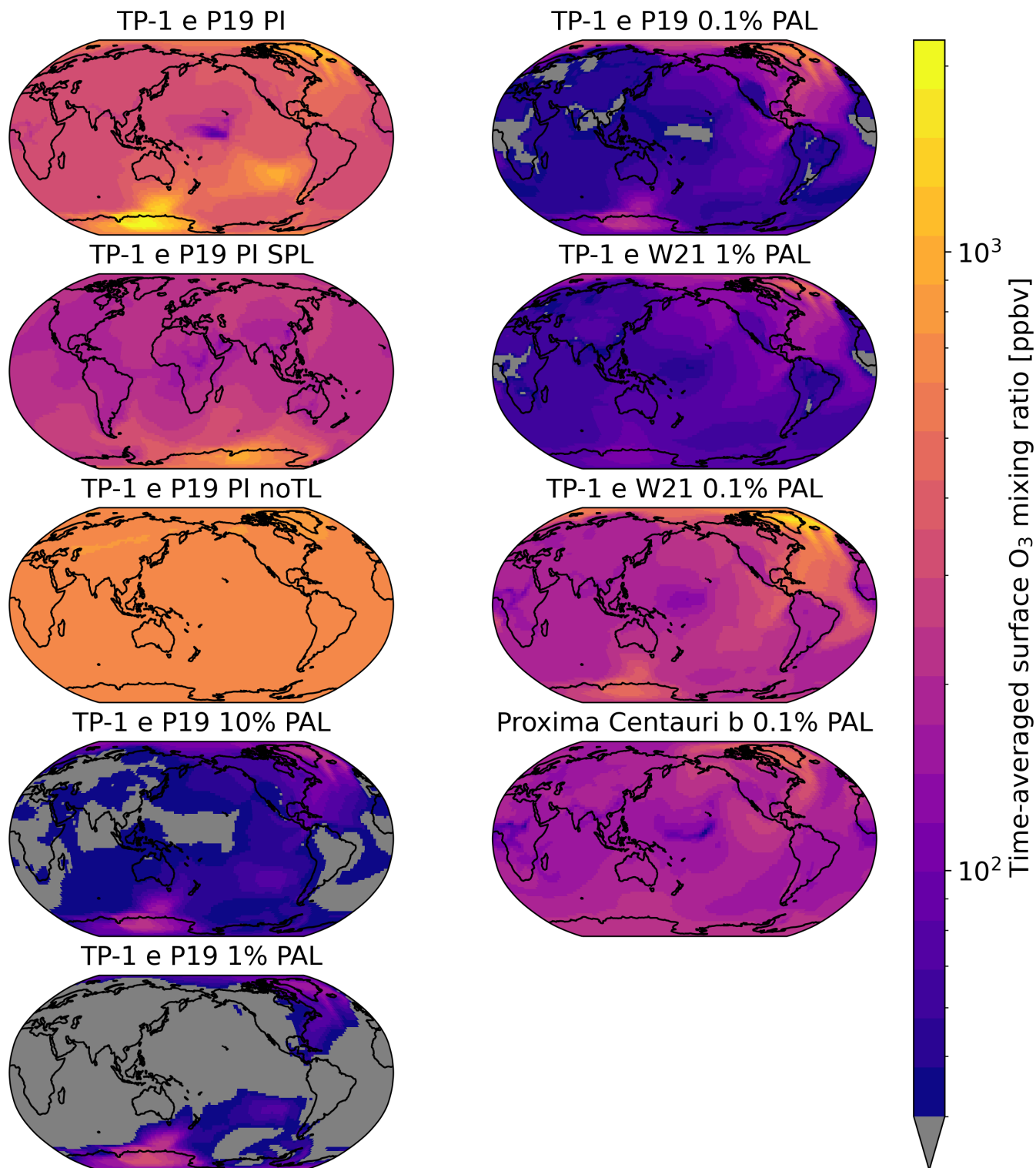


Figure 2. The surface mixing ratio of O_3 , in parts per billion by volume (ppbv), is displayed for the simulations in this work which have time-averaged surface O_3 mixing ratios exceeding 40 ppbv. This includes all TP-1 e P19 cases, the TP-1 e W21 1% PAL and 0.1% PAL simulations, and only a single Proxima Centauri b case (0.1% PAL). The PI cases start with an initial pre-industrial atmospheric composition. The PI case has the substellar point placed over the Pacific Ocean, the SPL case has it placed over Africa, and the noTL case is not tidally locked, so that the substellar point moves with time. PAL is the present atmospheric level of O_2 , which is a mixing ratio of 21% by volume. The TP-1 e P19 simulations have stronger incident ultraviolet radiation than the TP-1 e W21 simulations. See Table 1 for a more detailed description of the simulations. Grey indicates where the O_3 mixing ratio is below 40 ppbv and thus at “safe” levels, whilst the different shades of yellow-orange-purple indicate places that exceed 40 ppbv, i.e., these concentrations are known to be harmful to life on Earth. The colour map has a log scale which extends from 40 ppbv to 2200 ppbv.

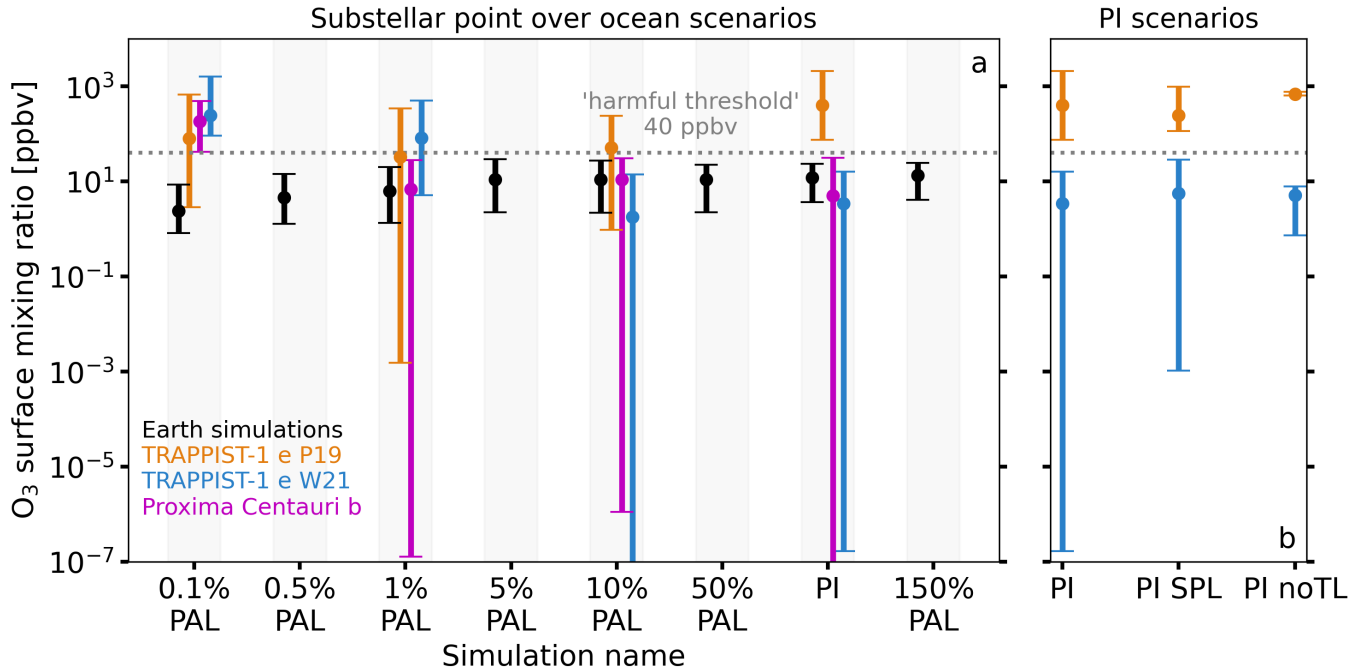


Figure 3. (a) Surface O_3 mixing ratios are presented for the tidally locked P19 (orange) and W21 (blue) TP-1 e simulations, and the PCb simulations (magenta). All of these simulations have the substellar point placed over ocean. The dots show the mean mixing ratio, whilst the top bar shows the maximum, and the bottom bar shows the minimum surface O_3 mixing ratios. Also shown in black are the time-averaged O_3 mixing ratios of data taken from [Cooke et al. \(2022\)](#). The horizontal axis indicates the simulations with a fixed O_2 mixing ratio at the lower boundary, such that the horizontal ticks are categories rather than absolute values (the values are offset from each other for clarity). The grey dotted line indicates the 40 ppbv ‘harmful threshold’, above which O_3 surface mixing ratios are considered dangerous to some forms of life on Earth. (b) The pre-industrial scenarios are compared in the TP-1 e simulations. These include the substellar point over ocean (PI), over land (PI SPL), and the non-tidally locked cases (PI noTL).

have a smaller range than both of the PI tidally locked cases, similar to the Earth simulations. These results imply that surface topography, the rotation rate, whether or not a diurnal cycle exists, and the position of the substellar point, will be important for modulating surface concentrations of biologically toxic gases such as O_3 . For the PCb scenarios, the PCb 0.1% PAL case reaches the largest O_3 mixing ratio of 466 ppbv, and everywhere has mixing ratios exceeding 40 ppbv. None of the WACCM6 Earth simulations from [Cooke et al. \(2022\)](#) have time-averaged O_3 mixing ratios at dangerous levels which is to be expected because industrial pollutants were not included in the simulations. If pollutants were included near urban areas, for instance, then harmful O_3 levels would be localised, rather than on a planetary scale. The simulations which have surface O_3 concentrations the most toxic to life are the PI, PI SPL, and PI noTL simulations with the P19 assumed spectrum. Quantitatively, this corresponds to the simulations where the global mean stratospheric O_3 number density exceeds 7×10^{18} molecules m^{-3} . All simulations with O_2 concentrations at 0.1% PAL have toxic mixing ratios exceeding 400 ppbv.

3.2. Cause of ozone production at the surface

It is important to state here that initially in the simulations, O_3 was present in Earth-like quantities throughout the troposphere, and no toxic concentrations existed at the start of the tidally locked simulations. The O_3 profile depends on UV radiation, O_2 number density, O_3 production rates, O_3 loss, and the transport of O_3 . Fig. 4 shows the photolysis rates of O_2 leading to O production (reactions 1 and 2), the photolysis rates of O_3 leading to O production (reactions 5 and 6), the production rates of O_3 (reaction 3), and the O_3 number density in each simulation. These quantities are important for understanding where O_3 is produced, and its resulting number density. O_2 has an approximately constant mixing ratio up until the homopause where gases start to diffusively separate, but in contrast, the mixing ratio of O increases with altitude until the homopause.

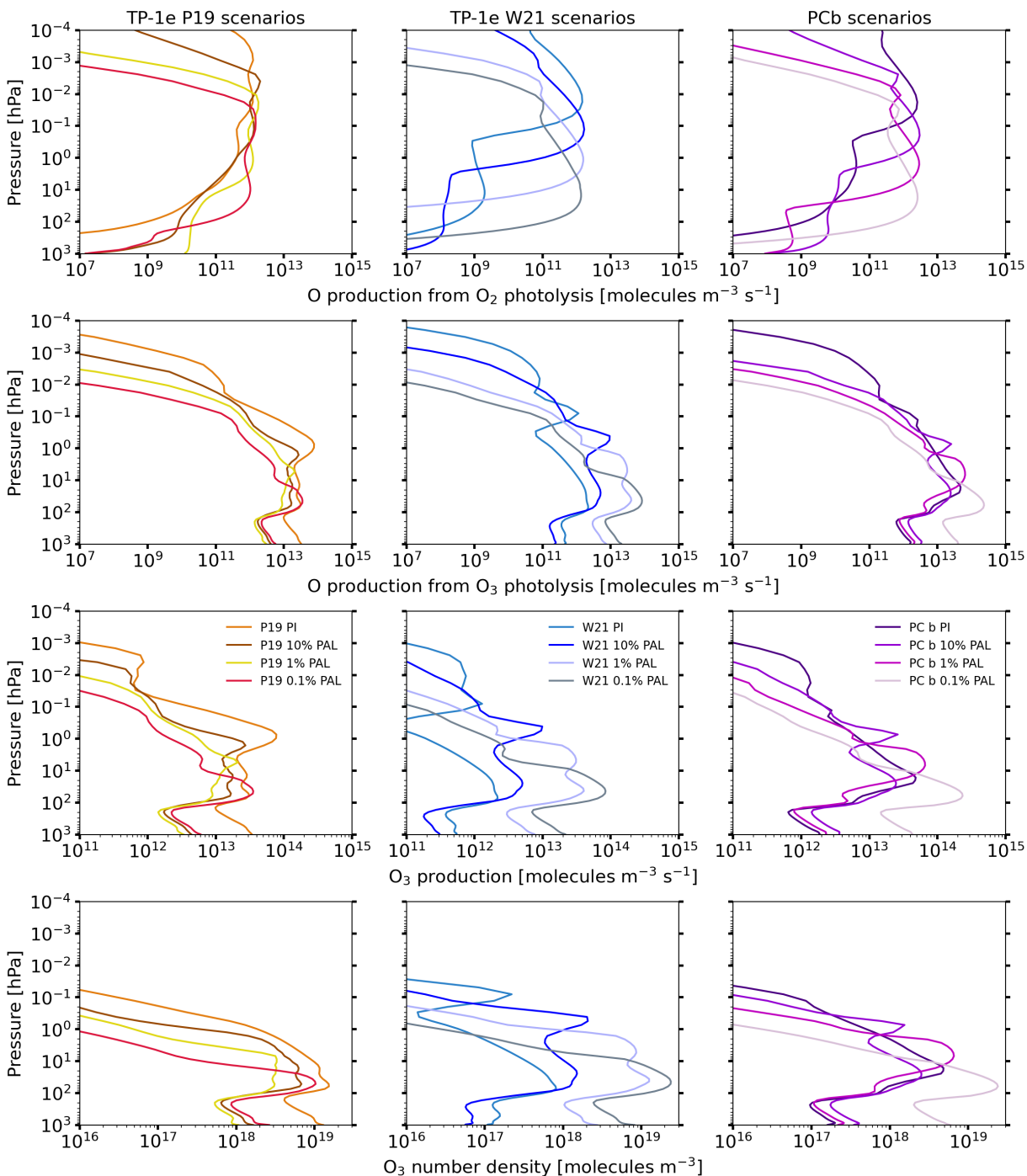


Figure 4. The production of O from O₂ photolysis (top row) and O₃ photolysis (second row) are shown against pressure, with O₃ production (third row) and O₃ number density also shown (bottom row). All profiles are time-averaged global means. The TP-1e PI, 10% PAL, 1% PAL, and 0.1% PAL simulations are shown for both the TP-1 e P19 (orange, brown, yellow, and red, respectively) and TP-1 e W21 (light blue, blue, lilac, and grey, respectively) stellar spectra in the left and middle columns, respectively. The right column show the PCb PI (indigo), 10% PAL (violet), 1% PAL (magenta), and 0.1% PAL (light pink) simulations.

In the W21 simulations, as O₂ decreases, the total amount of O₃ in the atmosphere, and at the surface, increases. The opposite is generally true in the P19 simulations, although there is an increase in surface O₃ between 1% PAL and 0.1% PAL. This difference between the P19 and W21 scenarios occurs due to the weak UV radiation in the W21

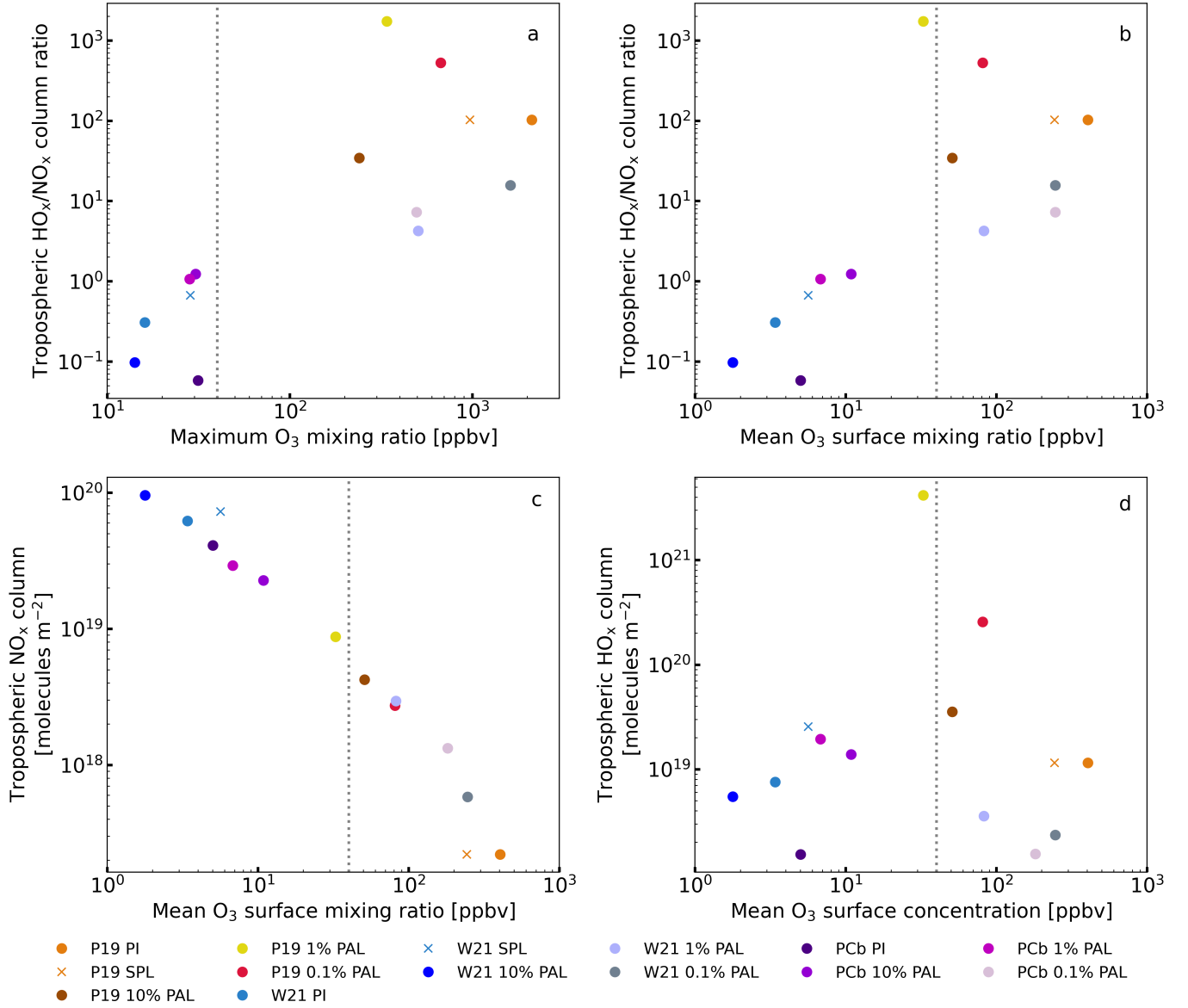


Figure 5. The tropospheric HO_x/NO_x column ratio is shown against the maximum and mean surface O_3 mixing ratio in each tidally locked simulation in panel **a** and **b**, respectively. The tropospheric NO_x and HO_x columns are shown against the mean O_3 surface mixing ratio in panel **c** and **d**, respectively. The grey vertical dotted lines show the 40 ppbv cut off for harmful O_3 levels. The tropospheric column is calculated as the column abundance of molecules between 120 hPa and the surface. Its units are molecules m^{-2} .

simulations, and the pressure dependency on the reaction which produces O_3 (reaction 3). When the peak of O_2 photolysis occurs at higher altitudes and thus lower pressure, then O does not react with O_2 as quickly to produce O_3 compared to the rate lower in the atmosphere where the density of the third body, M , is higher. In the P19 cases, whilst the UV can penetrate deeper into the atmosphere when the concentration of O_2 is reduced in the simulations, the availability of O_2 becomes the limiting factor for the production of O_3 , instead of UV radiation. In the PCb cases, there is an intermediate amount of UV radiation compared to the P19 and W21 TP-1 e cases. These PCb cases follow the same trend to the TP-1 e W21 scenarios, with the surface O_3 increasing as O_2 is reduced.

The destruction of O_3 plays an important role in these atmospheres too. Photolysis of O_3 is not counted as a loss of O_3 , because the O produced quickly cycles back to produce O_3 . The peak in O_2 photolysis, O_3 production, and O_3 number density, occurs in each simulation at pressures less than 100 hPa (above the troposphere). O_3 formation also

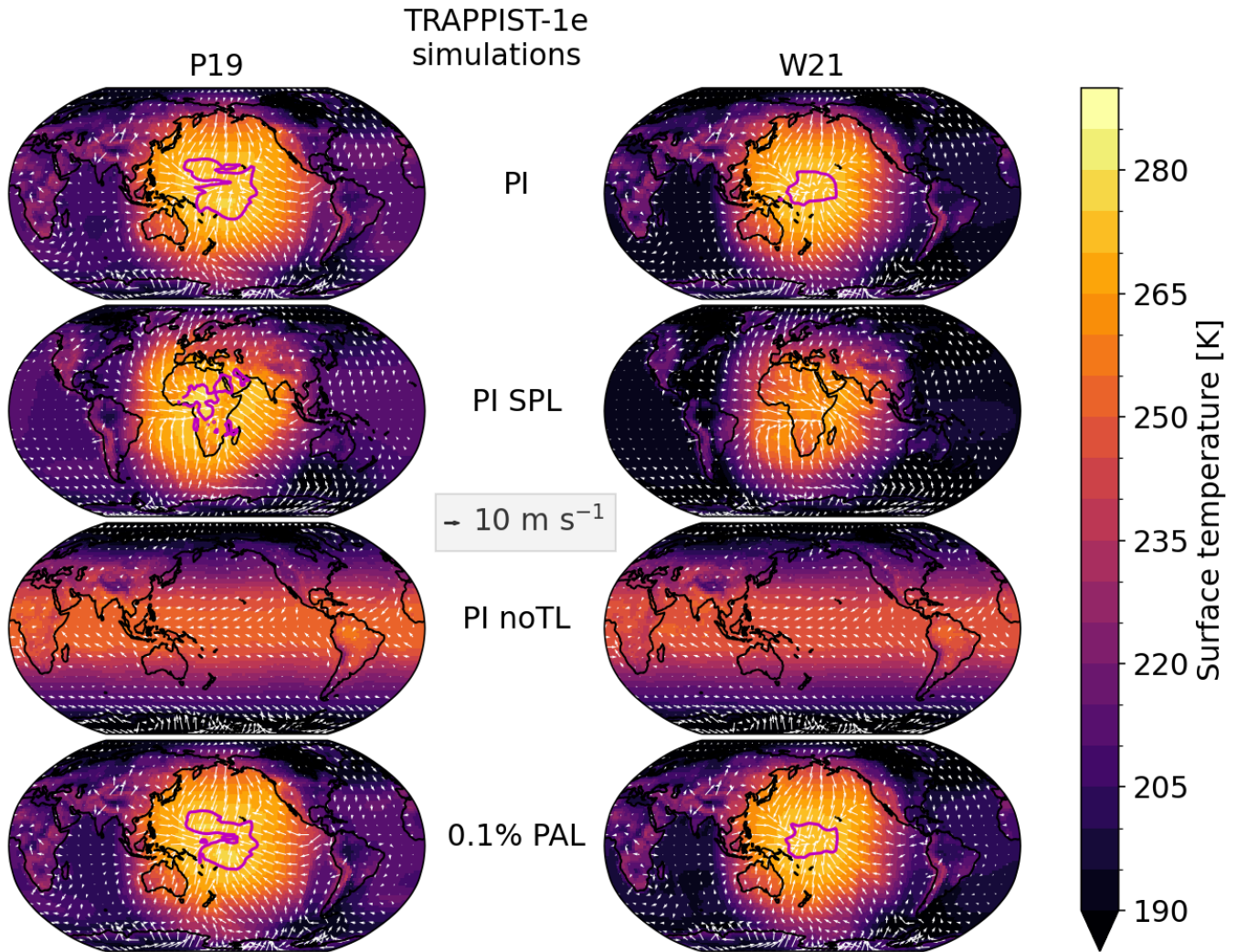


Figure 6. The surface temperature is displayed for the twelve TP-1 e simulations used in this work. The left column shows the P19 simulations and the right column shows the W21 simulations. From top to bottom: PI, PI SPL, PI noTL, and the 0.1% PAL simulations are displayed. White arrows indicate the magnitude and direction of the surface winds. The magenta contours show surface temperatures of 273 K. The 10% PAL and 1% PAL simulations are not shown for brevity, but their surface temperatures are very similar to the PI and 0.1% PAL cases. For scale, a 10 m s⁻¹ arrow is shown in the middle of the figure.

takes place in the troposphere because O₃ photolysis there is fast due to O₃ being present in relatively high quantities. O₃ is being destroyed (by HO_x and NO_x catalytic cycles) and remade in the troposphere, but compared to above the troposphere, its production via O₂, CO₂, NO₂, or H₂O photolysis is significantly slower. In the simulations that have toxic quantities of O₃, tropospheric destruction of O₃ is dominated by HO_x catalytic cycles rather than NO_x catalytic cycles. When O₃ is below harmful levels, NO_x catalytic cycles (predominantly NO and NO₂) dominate over HO_x catalytic cycle destruction of O₃. In other words, when NO and NO₂ are significantly depleted in the troposphere, O₃ is able to accumulate to harmful levels. The tropospheric column amount of NO_x exhibits negative correlation with the mean surface O₃ mixing ratio, as shown in Fig. 5. Therefore, the smog mechanism is not the reason for harmful levels of O₃, in contrast to modern day Earth.

The atmospheric temperatures and dynamics influence the abundance and distribution of O₃. Fig. 6 shows the surface temperatures (colour map) and surface winds (arrows) in the TP-1 e models, with Fig. 7 showing the same in the PCb models. Several TP-1 e tidally locked simulations have substellar points with temperatures above 273 K, and surface winds converging towards this point (associated with the day-side upwelling at the sub-stellar point),

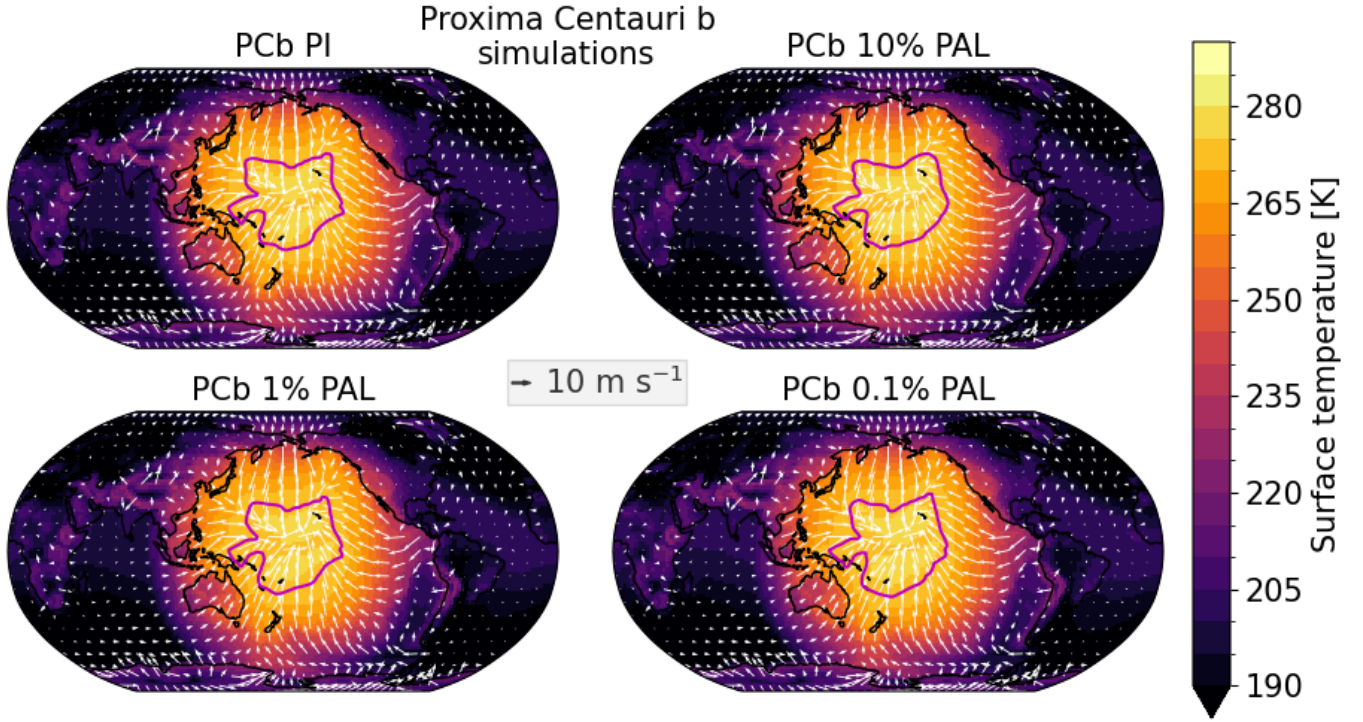


Figure 7. The surface temperature is displayed for the four PCb simulations used in this work: PCb PI (top left), PCb 10% PAL (top right), PCb 1% PAL (bottom left), PCb 0.1% PAL (bottom right). White arrows indicate the magnitude and direction of the surface winds. The magenta contours show surface temperatures of 273 K. For scale, a 10 m s^{-1} arrow is shown in the middle of the figure.

with some of the lowest surface mixing ratios also found near the substellar point. Away from the substellar point, temperatures drop below freezing and can be as low as 170 K on the nightside. The PCb cases have similar surface temperatures and winds because the total irradiance is quantitatively similar to the TP-1 e scenarios ($0.65 S_0$ versus $0.66 S_0$). The cold temperatures result in reduced destruction from catalytic cycles (see reaction 11) which proceed slower at lower temperatures (e.g., from HOx and NOx families), allowing O_3 to persist in relatively high quantities.

Fig. 8 shows the dry deposition flux of O_3 for some of the TRAPPIST-1 e simulations and the Earth PI simulation, and Table 2 shows the global mean dry deposition flux for the Earth PI, TRAPPIST-1 e, and Proxima Centauri b simulations. Dry deposition over snow and ice is slow compared to that over other surfaces (Wesely & Hicks 2000; Helmig et al. 2007; Barten et al. 2023). Additionally, marine surface deposition is slower than land deposition when plant stomata are available to take up O_3 (Ainsworth et al. 2012). If surface plants do not exist or have died from prolonged O_3 exposure (Rich 1964; Bytnerowicz et al. 1993; Sandermann Jr 1996; Rao & Davis 2001; Ramya et al. 2023), then dry deposition would occur more slowly, which results in even more O_3 build-up. Even if there are no surface or gaseous molecules for O_3 to interact with, the surface thermal decomposition of O_3 can take place and its importance may vary depending on the surface type, although this process is currently not sufficiently understood (Fowler et al. 2009; Clifton et al. 2020). The Earth PI simulation has a global mean dry deposition flux of $1.6 \times 10^{-11} \text{ kg m}^{-2} \text{ s}^{-1}$. All TRAPPIST-1 e and Proxima Centauri b simulations have reduced loss rates when compared to this, apart from the P19 PI, W21 1% PAL, W21 0.1% PAL and PCb 0.1% PAL simulations. Despite these cases having relatively high rates of dry deposition, all retain harmful concentrations of surface O_3 . For the Earth PI case, most O_3 is deposited over land (see Fig. 8). For the exoplanet simulations, the majority of O_3 is deposited near the substellar point, regardless of whether it is placed over land or ocean. The dry deposition flux around the substellar point contributes to the relatively reduced O_3 concentrations at the substellar point (e.g., see the P19 10% and 0.1% PAL simulations and W21 1% PAL and 0.1% PAL simulations in Fig. 2). The noTL cases have globally-averaged dry deposition rates that are slower than their PI tidally locked counterparts by a factor of 236 and 20 for the W21 and P19 scenarios, respectively.

To summarise the O₃ distribution in the simulations, O₃ is made primarily in the middle atmosphere on the modelled dayside and the O₃ column maximises at the poles (Cooke et al. 2023). O₃ loss on the nightside and at the poles is slower than the dayside due to relatively low temperatures and a lack of photolysis producing the molecules that become involved in O₃ destroying catalytic cycles. O₃ is lost at the surface due to dry deposition, but the flux is not large enough to mitigate for the dangerous concentrations of O₃. As an example, in the P19 PI case, the global mean dry deposition flux increases by ≈ 4.3 times greater than the Earth PI case, with a corresponding increase in surface O₃ concentrations of ≈ 33.7 . In the tidally locked cases, the O₃ chemical loss rate at the surface is approximately 2 – 29 times less than the peak stratospheric loss rate. Surface winds (of order 10 m s⁻¹), which are much stronger than vertical winds (of order 0.1 m s⁻¹), transport O₃ across the surface.

We hypothesise that O₃ is transported from where it is produced in the dayside stratosphere to the nightside and towards the poles as discussed in Braam et al. (2023), who simulated Proxima Centauri b assuming an initial condition of a modern-Earth atmosphere. The difference between our work and Braam et al. (2023) is, in several of our simulations, O₃ accumulates to harmful and lethal quantities. With loss processes in the troposphere less effective than in the stratosphere, the lifetime of surface O₃ increases and enables a build-up of toxic O₃ levels. The atmospheric transport throughout the entire atmosphere will be explored in a follow-up paper to confirm whether such a scenario is occurring in the simulations.

4. DISCUSSION

4.1. Prior results for toxic levels of ozone

As far as can be discerned from the presented data (e.g. globally averaged vertical profiles), other 3D simulations of oxygenated exoplanets (Proedrou & Hocke 2016; Way et al. 2017; Chen et al. 2019; Yates et al. 2020), excluding Braam et al. (2022), have not produced surface O₃ mixing ratios above 40 ppbv. This is likely due to the investigated scenarios which differ between each work, although model differences will be important (Ji et al. 2023; Ji et al. 2024). Figure 5 in Braam et al. (2022) shows dayside mixing ratios of O₃ reaching ≈ 45 ppbv at the surface. It is worth noting here that all of these studies, including our simulations, assume a surface pressure of 1 bar (1,000 hPa), so

Table 2. The time-averaged and global mean dry deposition flux of O₃ is given in terms of kg m⁻² s⁻¹, for all the exoplanet simulations used in this work, as well as the Earth PI simulation. Dry deposition is a sink for atmospheric surface O₃. The time-averaged and global mean O₃ surface mixing ratios are given. The fraction of the surface where O₃ concentrations are under 40 ppbv and thus considered “safe” is given for each simulated exoplanet scenario. The O₃ concentrations vary every calendar month, so the fraction is given as a range over a 1-year period and as a percentage. Additionally, the global mean O₃ column is given in Dobson Units (DU), where 1 DU is equal to 2.69×10^{20} molecules m⁻².

| Simulation | O ₃ dry deposition flux [kg m ⁻² s ⁻¹] | O ₃ surface mixing ratio [ppbv] | Fraction of surface with O ₃ mixing ratios < 40 ppbv | O ₃ column [DU] |
|--------------|--|--|---|----------------------------|
| Earth PI | 2.1×10^{-11} | 12 | N/A | 297 |
| W21 PI | 1.0×10^{-12} | 3 | 100 – 100% | 53 |
| W21 PI noTL | 4.3×10^{-15} | 5 | 100 – 100% | 46 |
| W21 PI SPL | 1.3×10^{-14} | 6 | 100 – 100% | 54 |
| W21 10% PAL | 6.2×10^{-13} | 2 | 100 – 100% | 154 |
| W21 1% PAL | 1.8×10^{-11} | 82 | 1 – 4% | 901 |
| W21 0.1% PAL | 4.9×10^{-11} | 246 | 0 – 0% | 1227 |
| P19 PI | 9.1×10^{-11} | 404 | 0 – 0% | 1289 |
| P19 PI noTL | 4.5×10^{-12} | 692 | 0 – 0% | 1245 |
| P19 PI SPL | 4.3×10^{-11} | 243 | 0 – 0% | 1098 |
| P19 10% PAL | 1.2×10^{-11} | 51 | 12 – 44% | 498 |
| P19 1% PAL | 6.3×10^{-12} | 31 | 75 – 83% | 260 |
| P19 0.1% PAL | 1.5×10^{-11} | 81 | 4 – 9% | 407 |
| PCb PI | 1.7×10^{-12} | 5 | 99 – 100% | 179 |
| PCb 10% PAL | 4.0×10^{-12} | 11 | 100 – 100% | 134 |
| PCb 1% PAL | 2.2×10^{-12} | 7 | 100 – 100% | 256 |
| PCb 0.1% PAL | 4.6×10^{-11} | 203 | 0 – 1% | 790 |

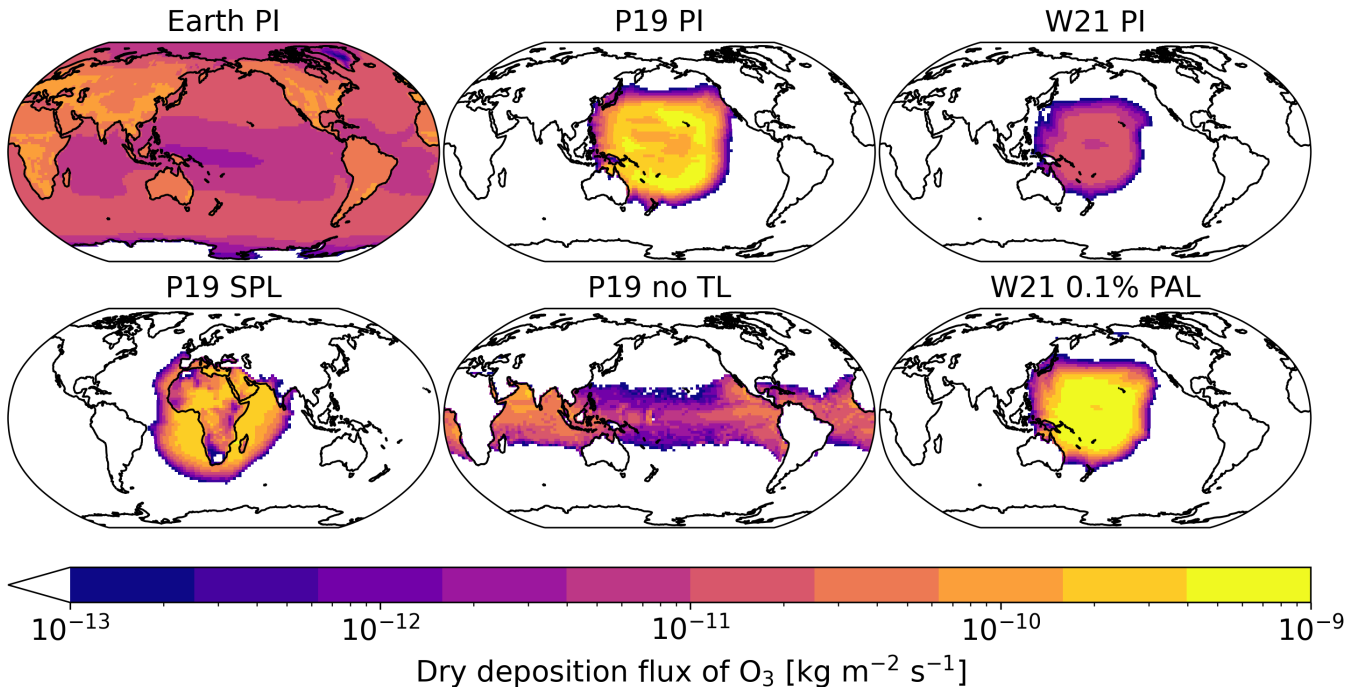


Figure 8. The dry deposition flux of O₃, given in terms of kg m⁻² s⁻¹, is plotted for six simulations: The Earth PI simulation, the TRAPPIST-1 e P19 PI, SPL, noTL, and W21 PI and 0.1% PAL simulations. Yellow indicates relatively large amounts of dry deposition, whilst red indicates relatively low amounts. The white areas indicate regions where the dry deposition flux of O₃ is below 10⁻¹³ kg m⁻² s⁻¹.

that a mixing ratio of 40 ppbv at 1,000 hPa surface pressure corresponds to a number density of 1.0×10^{18} molecules m⁻³ at 288 K. [Chen et al. \(2021\)](#) used WACCM4 and [Ridgway et al. \(2023\)](#) used the UM (two 3D chemistry-climate models) to investigate the impact of flares and coronal mass ejections on terrestrial exoplanets. The flares significantly perturbed O₃ concentrations⁵, but the changes were in the middle and upper atmosphere and the flares did not cause surface concentrations to exceed 40 ppbv. However, there could be specific cases where flares act to increase O₃ surface concentrations to harmful levels, likely depending on the atmospheric properties, incoming flare strength, and flare frequency.

1D photochemical models have also simulated the impact of flares, coronal mass ejections, and cosmic rays on atmospheric chemistry. The calculations in [Segura et al. \(2010\)](#), [Grenfell et al. \(2012\)](#), [Tabataba-Vakili et al. \(2016\)](#), and [Tilley et al. \(2019\)](#), did not demonstrate surface O₃ mixing ratios reaching biologically toxic quantities. The same is true for abiotic O₂ production simulations ([Segura et al. 2007](#); [Harman et al. 2015, 2018](#)), although it is unclear in the 100 bar atmosphere from [Schwieterman et al. \(2016\)](#) because surface O₃ mixing ratios are not shown (their figure 1), but O₃ is at 1 ppbv by 10 km and its mixing ratio is strongly decreasing with decreasing height. Other 1D photochemical modelling results for habitable zone exoplanets have shown that O₃ mixing ratios may exceed harmful levels ([Kozakis et al. 2018](#); [Fauchez et al. 2019](#); [Kaltenegger et al. 2020](#); [Kopparapu et al. 2021](#)). For example, [Kozakis et al. \(2018\)](#) used a 1D photochemical model (EXO-Prime; [Kaltenegger & Sasselov 2010](#)) to simulate Earth-like exoplanets with various surface pressures of 0.3, 1.0, 1.5, and 2.0 bar, orbiting white dwarf stars (stellar effective temperatures of 4000, 5000, and 6000 K). Almost all simulations had surface O₃ below the 40 ppbv threshold, with only a single simulation (0.3 bar surface pressure and 4000 K stellar effective temperature) exceeding it. However, if it is the concentration (number of molecules per unit volume), rather than the mixing ratio (fractional concentration), which is important, one must take into account the surface density of the atmosphere. Using this criterion, a few more simulations from [Kozakis et al. \(2018\)](#) would be close to 1.0×10^{18} O₃ molecules m⁻³ and therefore potentially dangerous to any surface life present. This was the case for simulated atmospheres around white dwarf stars, however,

⁵ The amount of atmospheric O₃ decreased by a factor of 3 in [Chen et al. \(2021\)](#) for active M dwarf stars, whereas total atmospheric O₃ increased by up to a factor of 20 in [Ridgway et al. \(2023\)](#).

the 1 bar atmospheres in [Kozakis & Kaltenecker \(2020\)](#) which were simulated around red giant stars did not surpass dangerous surface O_3 concentrations. Regarding smog (see Section 1 and Reactions 7 – 9), [Kopparapu et al. \(2021\)](#) used the 1D photochemical model which is part of ‘Atmos’ (see [Arney et al. 2016](#); [Arney 2019](#)) to simulate varying surface-to-atmosphere fluxes of NO_2 to test whether it could be used as a signature that extraterrestrial technology existed on an exoplanet. In two simulations (using a Sun-like star and a K6V star with $20\times$ the present Earth flux of NO_2), the surface O_3 mixing ratios were ≈ 90 and ≈ 100 ppbv, respectively. Alongside modern day pollution on Earth due to NO_x emissions from vehicles, this study by [Kopparapu et al. \(2021\)](#) demonstrates that the surface fluxes of molecules will be important for determining whether ground level O_3 concentrations reach concerning levels for life. [Fauchez et al. \(2019\)](#) simulated the habitable zone exoplanets TRAPPIST-1 e, f, and g, using the 3D model LMD-G and then performed terminator photochemistry simulations with Atmos. The surface O_3 concentrations are < 40 ppbv for TRAPPIST-1 e, but are ~ 60 ppbv and ~ 120 ppbv for TRAPPIST-1 f and g, respectively. In their simulations, surface O_3 increases with decreasing illumination. The simulations presented here predict, for the P19 PI case, the highest ozone surface concentrations (7.8×10^{19} molecules m^{-3}) compared with other results for exoplanets simulated in the literature.

WACCM6 predicts lower concentrations of O_3 for various oxygenation states (0.1 – 150% PAL) for Earth when compared to 1D models ([Cooke et al. 2022](#); [Ji et al. 2023](#)), so there is the question of why it now predicts higher concentrations of O_3 when compared to 1D models for M dwarf stars. There will likely be many reasons the results differ (e.g., see [Ji et al. 2023](#)), but we suspect that the main causes are differences in atmospheric transport and temperatures. The atmospheric temperatures in [Kozakis et al. \(2022\)](#) with the M5V star are warmer below 30 km when compared to the WACCM6 simulations. The same is true in the M3V and M8V simulations of [Rugheimer & Kaltenecker \(2018\)](#), the GJ 436 and GJ 876 simulations in [Rugheimer et al. \(2015\)](#), the [Gebauer et al. \(2018\)](#) simulations around AD Leo (M3.5V), the TRAPPIST-1 e simulations in [Lin et al. \(2021\)](#), the Proxima Centauri b simulations in [Scheucher et al. \(2020\)](#), and the 1 bar habitable Proxima Centauri b simulations in [Meadows et al. \(2018\)](#). Note that the desiccated Proxima Centauri b atmospheres in [Meadows et al. \(2018\)](#) do have harmful levels of O_3 , but these would not be considered habitable due to the lack of H_2O .

As an example of the temperature differences, global mean surface temperatures are approximately 220 – 230 K in the WACCM6 tidally locked simulations, compared to a surface temperature of ≈ 310 K in [Kozakis et al. \(2022\)](#), 260 – 280 K in [Scheucher et al. \(2020\)](#), and 273 K in [Meadows et al. \(2018\)](#). This means that below 30 km, where most of the atmospheric O_3 resides, loss rates will be slower and formation will be faster when compared to the 1D models. Furthermore, in 1D models, there is constant illumination, but in 3D models, O_3 is transported to the nightside (where there is no direct starlight) and down to the surface ([Braam et al. 2023](#)). The TRAPPIST-1 e 1D photochemical simulations in [Pidhorodetska et al. \(2020\)](#) used temperature and pressure profiles from 3D simulations of TRAPPIST-1 e ([Fauchez et al. 2019](#)). Here, the deviations from our results may be due to the synthetic BT-Settl spectrum (a model of stellar atmospheres; [Rajpurohit et al. 2013](#)) used by [Pidhorodetska et al. \(2020\)](#), and the fact that photochemistry was performed at the terminator. Between all of these simulations, there will be differences in photochemical cross sections and chemical schemes, as well as the UV spectra used and the total instellation, but temperatures and transport may largely explain the substantial discrepancies both in predicted surface O_3 , and O_3 columns, when compared to similar 1D model simulations.

With regards to why WACCM6 predicts higher surface concentrations of O_3 compared to the Unified Model will require a detailed intercomparison. For now, we speculate at least one difference is the use of a slab ocean with no ice formation in the Unified Model, such that O_3 will be lost in greater numbers on the nightside than would occur in reality. When simulating Proxima Centauri b with a slab ocean, [Yates et al. \(2020\)](#) and [Braam et al. \(2022\)](#) assumed a dry deposition velocity of 0.05 cm s^{-1} based on previous work ([Ganzeveld & Lelieveld 1995](#); [Giannakopoulos et al. 1999](#)). The global mean dry deposition velocities for O_3 in our tidally locked ocean substellar point cases are approximately 4 times slower, and slower still when considering the “noTL” and “SPL” cases. O_3 dry deposition depends on multiple interlinked parameters which are poorly known ([El-Madany et al. 2017](#)), so whether existing dry deposition parameterisations can be used for exoplanet simulations is not well known.

4.2. Modelling limitations

The model used for the atmospheric simulations is an important factor in these predictions because varying parameterisations and chemical schemes will impact the results. WACCM6 is a model that is tuned to Earth’s atmosphere, land, ice and ocean. WACCM6 accounts for scattering longward of 200 nm, but it doesn’t account for scattering in

the Schumann-Runge bands (175 – 192 nm; these wavelengths photolyse O_2 above ~ 80 km in Earth’s atmosphere), becoming pertinent for Earth-like simulations at O_2 mixing ratios of 1% PAL or less (Ji et al. 2023). In our simulations, WACCM6 accounts for absorption in the Schumann-Runge bands from O_3 , O_2 , CO_2 , and H_2O . The integrated flux in the Schumann-Runge Bands is 1.15, 656, and 26.6 times lower than Earth, for the TP-1 e P19, TP-1 e W21, and PCb cases, respectively. Even with the effects of scattering included, it seems still possible that harmful O_3 surface concentrations could form on the surface of terrestrial exoplanets because all of the P19 simulations have dangerous concentrations of surface O_3 . Moreover, the W21 simulations have a relatively low amount of radiation in the Schumann-Runge bands, yet toxic O_3 concentrations are found in the W21 1%, and 0.1% PAL cases. We tested these assumptions in the 0.1% PAL cases by reducing the incoming photon flux in the W21 and P19 spectra by a factor of 10^5 . The total integrated O_2 photolysis in the P19 0.1% PAL case reduced by a factor of 1.6, and in the W21 case the decrease was negligible. The decrease in O_2 photolysis in the P19 0.1% PAL case primarily takes place between 10 and 0.01 hPa. As seen from the results presented in figure 7 in Ji et al. (2023), scattering becomes important in the 0.1 – 10% PAL simulations at altitudes below 10 hPa. Therefore we expect our conclusions to be unaffected by including scattering in the Schumann-Runge band parameterisation in WACCM6; however, the test should still be done when that parameterisation is eventually updated.

4.3. Atmospheric evolution

We have assumed planetary conditions based on the last 2.4 billion years of Earth’s history, where the atmospheric pressure has been ~ 1 bar and atmospheric O_2 has varied between $1000\times$ less than the present atmospheric level to $\sim 1.5\times$ greater (Large et al. 2019; Catling & Zahnle 2020; Steadman et al. 2020; Lyons et al. 2021). However, for a habitable zone tidally locked exoplanet around an M dwarf star, is such a scenario realistic?

Firstly, atmospheres with high O_2 , CO_2 , or H_2O mixing ratios and sufficient UV may develop an O_3 layer close to the surface because photodissociation could produce O_2 and O molecules which lead to O_3 formation. In previous work simulating a 1 bar atmosphere around the host star GJ 876, O_2 amounts comparable to the Proterozoic Earth were produced in abiotic scenarios (Domagal-Goldman et al. 2014; Tian et al. 2014). When CO_2 is photolysed it produces CO and O, but lightning flashes can produce NO, which can catalyse the recombination of CO and O (instead of O going on to produce O_2), meaning that abiotic O_2 may not increase to detectable levels (Harman et al. 2018). However, on some exoplanets lightning may not be sufficient to prevent O_2 build-up (Barth et al. 2024).

Oxygenic photosynthesis on Earth, utilising chlorophyll as a pigment, requires photosynthetically active radiation (PAR) between 400–700 nm (Alados et al. 1996). Due to the luminosity of M dwarf stars peaking at longer wavelengths when compared to the Sun, the availability of PAR may be lacking on habitable M dwarf exoplanets. Nevertheless, oxygenic photosynthesis is thought to be possible on exoplanets orbiting M dwarf stars (Gale & Wandel 2017; Claudi et al. 2020; Duffy et al. 2023), although some exoplanets may be limited by a lack of photons reaching the surface (Lehmer et al. 2018) and this could mean that anoxygenic photosynthesis (where oxygen is not a product of photosynthesis) is preferentially selected (Duffy et al. 2023). In particular, the results from Lingam & Loeb (2019) showed how planets orbiting stars with masses below $0.13 M_\odot$ may have difficulties in producing O_2 through oxygenic photosynthesis, with Proxima Centauri and TRAPPIST-1 falling under this limit. However, the results of Covone et al. (2021) contrasted to Lingam & Loeb (2019), and whilst TRAPPIST-1 f and g might be energy limited (Lehmer et al. 2018; Covone et al. 2021), TRAPPIST-1 e may be able to host an Earth-like biosphere. Furthermore, cyanobacteria can use radiation longward of 700 nm to photosynthesize (Gan & Bryant 2015; Claudi et al. 2020), and a recent study has also shown this in more complex vegetation (Zhen et al. 2022). A new metric quantifying the photo-absorption rate of photosynthetic pigments around different stars, suggests M8V stars could activate photosynthesis (Marcos-Arenal et al. 2022). Moreover, cyanobacteria can survive and photosynthesize in caves and under low light conditions (Hanelt et al. 1997; Behrendt et al. 2020; Jung et al. 2023). Regardless of the possibility of photosynthesis on M dwarfs, O_2 production needs to surpass O_2 sinks in order to produce an oxygenated atmosphere (Lehmer et al. 2018).

It is hypothesized that the oxidation of Earth’s lithosphere (the solid outer layer of a planet) occurred due to two primary factors: oxygenic photosynthesis from cyanobacteria over millions of years, and hydrogen escape to space resulting from water photolysis (Catling et al. 2001; Zahnle et al. 2013). Modelling an Earth-like planet orbiting the star AD-Leo (M3.5V), Gebauer et al. (2018) found that it may be possible for a Great Oxidation Event (see e.g., Lyons et al. 2014; Gumsley et al. 2017; Poulton et al. 2021) to occur earlier in the history of the modelled planet when compared to Earth. If O_2 increases and results in large amounts of O_3 at the surface, because O_3 is a strong oxidiser,

it could speed up the oxidation of Earth’s lithosphere, reducing the sinks of O_2 and further enabling the generation of an oxygenated atmosphere.

4.4. *Habitability feedback*

Continuing with this scenario in mind, there is the potential for biological feedback. Surface O_3 may build-up to toxic concentrations and kill organisms that produce O_2 on the surface, subsequently reducing the production of O_2 until O_3 reaches safe levels again. Even so, we argue here that O_3 could exceed lethal surface concentrations and a photosynthetic biosphere could still be safely present in the ocean and under ice.

Firstly, refuge from the dangerous O_3 concentrations may be found in any liquid water ocean present, because O_3 has low solubility in water (Egorova et al. 2015). Although it is possible for O_3 to form in water which is irradiated by the Sun (Lushchak 2011), O_3 then quickly decomposes. Additionally, for disinfection applications, O_3 has to be artificially inserted into water (e.g., via bubble diffusion; Wert et al. 2017) such that it seems unlikely that marine life would be adversely affected by high surface concentrations of O_3 in the air. The known effects of O_3 exposure on life are limited to observations of terrestrial organisms, and extraterrestrial organisms may adapt to survive in an atmosphere with high surface O_3 mixing ratios.

On Earth, phytoplankton blooms have been found under Arctic (Suzuki et al. 1997; Arrigo et al. 2012; Clement Kinney et al. 2020) and Antarctic sea ice (McMinn et al. 2007), algae are found at varying depths (Norris & Olsen 1991; Pritchard et al. 2013; Borlongan et al. 2017), and lichens (Kappen 1993), aquatic plants (Adams et al. 1974; Campbell et al. 2007), and seaweed (Ramus et al. 1976; Huovinen & Gómez 2013), can photosynthesize below the surface. The long day length during the summers at each pole on Earth can increase the rate of primary productivity (Henshaw & Laybourn-Parry 2002). Given phytoplankton’s contribution to roughly half of Earth’s primary productivity (Field et al. 1998) and the potential for subsurface photosynthesis on tidally locked exoplanets with constant day side illumination, significant oxygen accumulation may occur without surface life. The amount of ice coverage and available area of open ocean may limit the O_2 flux to the atmosphere, although gaseous diffusion through sea ice is possible (Delille et al. 2007; Loose et al. 2011; Loose et al. 2011; Bortkovskii 2012), just slower when compared to open water (Bortkovskii 2012).

In summary, whether due to biological or abiotic production, O_2 could be produced in quantities large enough to induce toxic concentrations of O_3 at the surface. If life is present on such a planet, there is then the potential for biogeochemical feedback as organisms are hindered or destroyed by O_3 . We encourage simulations of these scenarios using biogeochemical models to quantitatively determine the possible outcomes we have discussed.

4.5. *Future work*

Future work should aim to determine the parameter space (in UV irradiation, composition, and atmospheric pressure) for which detrimental levels of surface level O_3 may occur. Ideally, 1D photochemical models would be used for this as they are less computationally expensive than 3D models, and the use of 1D photochemical models is indeed a viable investigation for non-tidally locked exoplanets. However, for tidally locked exoplanets, where O_3 is transported to the nightside and shielded from destruction (Proedrou & Hocke 2016; Yates et al. 2020; Braam et al. 2023), 3D chemistry-climate models will be needed to predict where surface O_3 concentrations maximise due to atmospheric dynamics, and climatology from varied ocean and land configurations (Zhao et al. 2021; Macdonald et al. 2022). The ocean salinity could be varied to determine the affect on the sea ice distribution (Olson et al. 2022), which is important for habitability estimates and O_3 dry deposition calculations. Simulations where only the ocean model is changed between dynamic ocean, slab ocean with ice formation (e.g., Olson et al. 2022), and slab ocean without ice formation (e.g., Braam et al. 2022), would be useful to determine how important these factors are when considering toxic O_3 at the surface. Additionally, one could explore various topographies, gravitational accelerations, and several different atmospheric compositions (e.g., H_2O or CO_2 dominated). As the exoplanets simulated here have limited areas where surface temperatures are above 273 K (and some have no surface temperatures above 273 K), subsequent research could investigate the parameter space with warmer exoplanets to determine how surface O_3 concentrations are affected. Examples of other 3D models that could investigate this chemical phenomenon are LMD-G (Yassin Jaziri et al. 2022), ROCKE-3D (Way et al. 2017), and the Unified Model (Boutle et al. 2017). Once a chemical scheme is implemented, the LFRic-Atmosphere model could also be used (Sergeev et al. 2023).

The classical HZ depends on whether a planet can sustain surface liquid water, but the notion of a Habitable Zone for Complex Life (Schwieterman et al. 2019) is influenced by the presence of toxic gases. So far, the toxic gases that

have been suggested are carbon monoxide (CO) and relatively high concentrations of CO₂ (Schwieterman et al. 2019), as well as N₂ at high pressure (e.g., > 2 bar; Ramirez 2020). These molecules impede biochemical processes that may be unique to organisms on Earth. Resulting from its reactivity as a strong oxidant, O₃ could pose a more significant threat to extraterrestrial life. Therefore, based on our modelling work and the properties of O₃, we recommend that O₃ should now be added to the list of molecules that can influence the Habitable Zone for Complex Life.

5. CONCLUSIONS

This work used WACCM6 to simulate the climate of two exoplanets: TRAPPIST-1 e and Proxima Centauri b. For each exoplanet, we considered O₂ mixing ratios between 0.1% PAL and 100% PAL. Additionally, two different stellar spectra were used for the TRAPPIST-1 e cases to investigate the effect on surface O₃ due to their large differences in the strength of incoming UV radiation. In multiple simulations, surface concentrations of O₃ exceed 40 ppbv, with maximum time-averaged concentrations reaching up to 2200 ppbv in the TP-1 e P19 PI case. Such concentrations are harmful to life on Earth and may be potentially fatal through oxidative stress. In these simulated atmospheres, O₃ exists not as a pollutant, but as a consequence of the planetary atmospheric conditions, such as the 1,000 hPa surface pressure, the incoming UV strength and shape, and the O₂ number density vertical profile. Our work suggests the potential presence of toxic O₃ concentrations should be included when evaluating the habitability of an exoplanet.

The simulations examined in this exploratory work represent a small proportion of the parameter space in which atmospheres may form relatively high O₃ concentrations at the surface. Different planetary rotation rates, topography, atmospheric pressures, total irradiation and UV irradiation environments, as well as various chemical fluxes from the surface to the atmosphere, should all be explored. Upcoming work should consider the potential presence of high surface concentrations of O₃ when simulating oxygenated atmospheres. If O₃ is detected in any future observations of terrestrial exoplanet atmospheres, ascertaining the O₃ surface concentration should be incorporated into frameworks that aim to determine planetary habitability and decide on the most promising targets for follow-up observations (see e.g., Truitt et al. 2020; Méndez et al. 2021; Safonova et al. 2021). In practise, this will require a combination of planetary modelling, transmission and direct imaging spectra, as well as precise knowledge of the UV irradiation environment of the atmosphere. 3D chemistry-climate models are essential for understanding how transport can create areas with comparatively lower and thus safer O₃ concentrations. Just as on Earth, the entire surface does not need to be hospitable for life to flourish.

ACKNOWLEDGMENTS

We thank the two reviewers for their comments and helpful feedback which helped to improve the manuscript.

G.J.C. acknowledges the studentship funded by the Science and Technology Facilities Council of the United Kingdom (STFC; grant number ST/T506230/1). C.W. acknowledges financial support from the University of Leeds and from the Science and Technology Facilities Council (grant numbers ST/X001016/1 and MR/T040726/1). F.S.-M. acknowledges financial support from the University of Leeds and from the Science and Technology Facilities Council (grant number MR/T040726/1). This work was undertaken on ARC4, part of the High Performance Computing facilities at the University of Leeds, UK.

REFERENCES

- Adams, M. S., Titus, J., & McCracken, M. 1974, *Limnology and oceanography*, 19, 377
- Agol, E., Dorn, C., Grimm, S. L., et al. 2021, *PSJ*, 2, 1, doi: [10.3847/PSJ/abd022](https://doi.org/10.3847/PSJ/abd022)
- Ainsworth, E. A., Yendrek, C. R., Sitch, S., Collins, W. J., & Emberson, L. D. 2012, *Annual review of plant biology*, 63, 637
- Alados, I., Foyo-Moreno, I., & Alados-Arboledas, L. 1996, *Agricultural and Forest Meteorology*, 78, 121, doi: [10.1016/0168-1923\(95\)02245-7](https://doi.org/10.1016/0168-1923(95)02245-7)
- Arney, G., Domagal-Goldman, S. D., Meadows, V. S., et al. 2016, *Astrobiology*, 16, 873, doi: [10.1089/ast.2015.1422](https://doi.org/10.1089/ast.2015.1422)
- Arney, G. N. 2019, *ApJL*, 873, L7, doi: [10.3847/2041-8213/ab0651](https://doi.org/10.3847/2041-8213/ab0651)
- Arrigo, K. R., Perovich, D. K., Pickart, R. S., et al. 2012, *Science*, 336, 1408
- Atkinson, R. 2000, *Atmospheric Environment*, 34, 2063, doi: [10.1016/S1352-2310\(99\)00460-4](https://doi.org/10.1016/S1352-2310(99)00460-4)
- Avnery, S., Mauzerall, D. L., Liu, J., & Horowitz, L. W. 2011, *Atmospheric Environment*, 45, 2284, doi: [10.1016/j.atmosenv.2010.11.045](https://doi.org/10.1016/j.atmosenv.2010.11.045)

- Barten, J. G., Ganzeveld, L. N., Steeneveld, G.-J., et al. 2023, *Elem Sci Anth*, 11, 00086
- Barth, P., Stüeken, E. E., Helling, C., Schwieterman, E. W., & Telling, J. 2024, arXiv e-prints, arXiv:2402.13682, doi: [10.48550/arXiv.2402.13682](https://doi.org/10.48550/arXiv.2402.13682)
- Behrendt, L., Trampe, E. L., Nord, N. B., et al. 2020, *Environmental microbiology*, 22, 952
- Bell, M. L., Peng, R. D., & Dominici, F. 2006, *Environmental health perspectives*, 114, 532
- Borlongan, I. A., Nishihara, G. N., Shimada, S., & Terada, R. 2017, *Journal of applied phycology*, 29, 3077
- Bortkovskii, R. S. 2012, *Izvestiya Atmospheric and Oceanic Physics*, 48, 538, doi: [10.1134/S0001433812040044](https://doi.org/10.1134/S0001433812040044)
- Boutle, I. A., Mayne, N. J., Drummond, B., et al. 2017, *A&A*, 601, A120, doi: [10.1051/0004-6361/201630020](https://doi.org/10.1051/0004-6361/201630020)
- Braam, M., Palmer, P. I., Decin, L., Cohen, M., & Mayne, N. J. 2023, *MNRAS*, 526, 263, doi: [10.1093/mnras/stad2704](https://doi.org/10.1093/mnras/stad2704)
- Braam, M., Palmer, P. I., Decin, L., et al. 2022, *MNRAS*, 517, 2383, doi: [10.1093/mnras/stac2722](https://doi.org/10.1093/mnras/stac2722)
- Brasseur, G. P., & Solomon, S. 2005, *Aeronomy of the Middle Atmosphere: Chemistry and Physics of the Stratosphere and Mesosphere* (Springer)
- Brugger, B., Mousis, O., Deleuil, M., & Lunine, J. I. 2016, *ApJL*, 831, L16, doi: [10.3847/2041-8205/831/2/L16](https://doi.org/10.3847/2041-8205/831/2/L16)
- Butchart, N. 2014, *Reviews of geophysics*, 52, 157
- Bytnerowicz, A., Manning, W. J., Grosjean, D., et al. 1993, *Environmental Pollution*, 80, 301
- Campbell, S. J., McKenzie, L. J., Kerville, S. P., & Bité, J. S. 2007, *Estuarine Coastal and Shelf Science*, 73, 551, doi: [10.1016/j.ecss.2007.02.014](https://doi.org/10.1016/j.ecss.2007.02.014)
- Carone, L., Keppens, R., Decin, L., & Henning, T. 2018, *MNRAS*, 473, 4672, doi: [10.1093/mnras/stx2732](https://doi.org/10.1093/mnras/stx2732)
- Catling, D. C., & Zahnle, K. J. 2020, *Science Advances*, 6, eaax1420, doi: [10.1126/sciadv.aax1420](https://doi.org/10.1126/sciadv.aax1420)
- Catling, D. C., Zahnle, K. J., & McKay, C. P. 2001, *Science*, 293, 839
- Chameides, W. L., Lindsay, R. W., Richardson, J., & Kiang, C. S. 1988, *Science*, 241, 1473, doi: [10.1126/science.3420404](https://doi.org/10.1126/science.3420404)
- Chen, H., Wolf, E. T., Zhan, Z., & Horton, D. E. 2019, *ApJ*, 886, 16, doi: [10.3847/1538-4357/ab4f7e](https://doi.org/10.3847/1538-4357/ab4f7e)
- Chen, H., Zhan, Z., Youngblood, A., et al. 2021, *Nature Astronomy*, 5, 298, doi: [10.1038/s41550-020-01264-1](https://doi.org/10.1038/s41550-020-01264-1)
- Claudi, R., Alei, E., Battistuzzi, M., et al. 2020, *Life*, 11, 10, doi: [10.3390/life11010010](https://doi.org/10.3390/life11010010)
- Clement Kinney, J., Maslowski, W., Osinski, R., et al. 2020, *Journal of Geophysical Research (Oceans)*, 125, e2020JC016211, doi: [10.1029/2020JC016211](https://doi.org/10.1029/2020JC016211)
- Clifton, O. E., Fiore, A. M., Massman, W. J., et al. 2020, *Reviews of Geophysics*, 58, e2019RG000670, doi: [10.1029/2019RG000670](https://doi.org/10.1029/2019RG000670)
- Colose, C. M., Del Genio, A. D., & Way, M. J. 2019, *ApJ*, 884, 138, doi: [10.3847/1538-4357/ab4131](https://doi.org/10.3847/1538-4357/ab4131)
- Cooke, G., Marsh, D., Walsh, C., & Youngblood, A. 2023, arXiv preprint arXiv:2309.15239
- Cooke, G. J., Marsh, D. R., Walsh, C., Black, B., & Lamarque, J. F. 2022, *Royal Society Open Science*, 9, 211165, doi: [10.1098/rsos.211165](https://doi.org/10.1098/rsos.211165)
- Cooke, G. J., Marsh, D. R., Walsh, C., Rugheimer, S., & Villanueva, G. L. 2023, *MNRAS*, 518, 206, doi: [10.1093/mnras/stac2604](https://doi.org/10.1093/mnras/stac2604)
- Covone, G., Ienco, R. M., Cacciapuoti, L., & Inno, L. 2021, *MNRAS*, 505, 3329, doi: [10.1093/mnras/stab1357](https://doi.org/10.1093/mnras/stab1357)
- Del Genio, A. D., Way, M. J., Amundsen, D. S., et al. 2019, *Astrobiology*, 19, 99, doi: [10.1089/ast.2017.1760](https://doi.org/10.1089/ast.2017.1760)
- Delille, B., Jourdain, B., Borges, A. V., Tison, J.-L., & Delille, D. 2007, *Limnology and Oceanography*, 52, 1367, doi: [10.4319/lo.2007.52.4.1367](https://doi.org/10.4319/lo.2007.52.4.1367)
- Démare, F., Gibert, L., Creusot, P., Lapeyre, B., & Proffit, M. 2022, *Science of the Total Environment*, 827, 154342, doi: [10.1016/j.scitotenv.2022.154342](https://doi.org/10.1016/j.scitotenv.2022.154342)
- Des Marais, D. J., Harwit, M. O., Jucks, K. W., et al. 2002, *Astrobiology*, 2, 153, doi: [10.1089/15311070260192246](https://doi.org/10.1089/15311070260192246)
- Domagal-Goldman, S. D., Segura, A., Claire, M. W., Robinson, T. D., & Meadows, V. S. 2014, *ApJ*, 792, 90, doi: [10.1088/0004-637X/792/2/90](https://doi.org/10.1088/0004-637X/792/2/90)
- Duffy, C. D. P., Canchon, G., Haworth, T. J., et al. 2023, *MNRAS*, 526, 2265, doi: [10.1093/mnras/stad2823](https://doi.org/10.1093/mnras/stad2823)
- Egorova, G., Voblikova, V., Sabitova, L., et al. 2015, *Moscow University Chemistry Bulletin*, 70, 207
- El-Madany, T., Niklasch, K., & Klemm, O. 2017, *Atmosphere*, 8, 175, doi: [10.3390/atmos8090175](https://doi.org/10.3390/atmos8090175)
- Emmons, L. K., Schwantes, R. H., Orlando, J. J., et al. 2020, *Journal of Advances in Modeling Earth Systems*, 12, e2019MS001882, doi: [10.1029/2019MS001882](https://doi.org/10.1029/2019MS001882)
- Epelle, E. I., Macfarlane, A., Cusack, M., et al. 2023, *Chemical Engineering Journal*, 454, 140188
- . 2022, *Journal of Microbiological Methods*, 194, 106431
- Erickson, M. C., & Ortega, Y. R. 2006, *Journal of food protection*, 69, 2786
- Faria, J. P., Suárez Mascareño, A., Figueira, P., et al. 2022, *A&A*, 658, A115, doi: [10.1051/0004-6361/202142337](https://doi.org/10.1051/0004-6361/202142337)
- Faucher, T. J., Turbet, M., Villanueva, G. L., et al. 2019, *ApJ*, 887, 194, doi: [10.3847/1538-4357/ab5862](https://doi.org/10.3847/1538-4357/ab5862)
- Faucher, T. J., Turbet, M., Wolf, E. T., et al. 2020, *Geoscientific Model Development*, 13, 707, doi: [10.5194/gmd-13-707-2020](https://doi.org/10.5194/gmd-13-707-2020)

- Feng, Z., Xu, Y., Kobayashi, K., et al. 2022, *Nature Food*, 3, 47
- Field, C. B., Behrenfeld, M. J., Randerson, J. T., & Falkowski, P. 1998, *Science*, 281, 237, doi: [10.1126/science.281.5374.237](https://doi.org/10.1126/science.281.5374.237)
- Fontes, B., Cattani Heimbecker, A. M., de Souza Brito, G., et al. 2012, *BMC infectious diseases*, 12, 1
- Fowler, D., Pilegaard, K., Sutton, M. A., et al. 2009, *Atmospheric Environment*, 43, 5193, doi: [10.1016/j.atmosenv.2009.07.068](https://doi.org/10.1016/j.atmosenv.2009.07.068)
- Fowler, J., Haffert, S. Y., van Kooten, M. A. M., et al. 2023, arXiv e-prints, arXiv:2309.00725, doi: [10.48550/arXiv.2309.00725](https://doi.org/10.48550/arXiv.2309.00725)
- France, K., Loyd, R. O. P., Youngblood, A., et al. 2016, *ApJ*, 820, 89, doi: [10.3847/0004-637X/820/2/89](https://doi.org/10.3847/0004-637X/820/2/89)
- Froning, C. S., Kowalski, A., France, K., et al. 2019, *ApJL*, 871, L26, doi: [10.3847/2041-8213/aaffcd](https://doi.org/10.3847/2041-8213/aaffcd)
- Fu, Q., Solomon, S., Pahlavan, H. A., & Lin, P. 2019, *Environmental Research Letters*, 14, 114026, doi: [10.1088/1748-9326/ab4de7](https://doi.org/10.1088/1748-9326/ab4de7)
- Gaia Collaboration, Brown, A. G. A., Vallenari, A., et al. 2016, *A&A*, 595, A2, doi: [10.1051/0004-6361/201629512](https://doi.org/10.1051/0004-6361/201629512)
- Gale, J., & Wandel, A. 2017, *International Journal of Astrobiology*, 16, 1, doi: [10.1017/S1473550415000440](https://doi.org/10.1017/S1473550415000440)
- Gan, F., & Bryant, D. A. 2015, *Environmental microbiology*, 17, 3450
- Ganzeveld, L., & Lelieveld, J. 1995, *J. Geophys. Res.*, 100, 20,999, doi: [10.1029/95JD02266](https://doi.org/10.1029/95JD02266)
- Gao, P., Hu, R., Robinson, T. D., Li, C., & Yung, Y. L. 2015, *ApJ*, 806, 249, doi: [10.1088/0004-637X/806/2/249](https://doi.org/10.1088/0004-637X/806/2/249)
- Garcia, R. R., & Randel, W. J. 2008, *Journal of Atmospheric Sciences*, 65, 2731, doi: [10.1175/2008JAS2712.1](https://doi.org/10.1175/2008JAS2712.1)
- Gebauer, S., Grenfell, J. L., Lehmann, R., & Rauer, H. 2018, *Astrobiology*, 18, 856, doi: [10.1089/ast.2017.1723](https://doi.org/10.1089/ast.2017.1723)
- Gettelman, A., Mills, M. J., Kinnison, D. E., et al. 2019, *Journal of Geophysical Research (Atmospheres)*, 124, 12,380, doi: [10.1029/2019JD030943](https://doi.org/10.1029/2019JD030943)
- Giannakopoulos, C., Chipperfield, M. P., Law, K. S., & Pyle, J. A. 1999, *J. Geophys. Res.*, 104, 23,761, doi: [10.1029/1999JD900392](https://doi.org/10.1029/1999JD900392)
- Giese, A. C., & Christensen, E. 1954, *Physiological zoology*, 27, 101
- Gonçalves, A. A., & Gagnon, G. A. 2011, *Ozone: Science & Engineering*, 33, 345
- Greene, T. P., Bell, T. J., Ducrot, E., et al. 2023, *Nature*, 618, 39, doi: [10.1038/s41586-023-05951-7](https://doi.org/10.1038/s41586-023-05951-7)
- Grenfell, J. L., Stracke, B., Patzer, B., Titz, R., & Rauer, H. 2006, *International Journal of Astrobiology*, 5, 295, doi: [10.1017/S1473550406003478](https://doi.org/10.1017/S1473550406003478)
- Grenfell, J. L., Griebmeier, J.-M., von Paris, P., et al. 2012, *Astrobiology*, 12, 1109, doi: [10.1089/ast.2011.0682](https://doi.org/10.1089/ast.2011.0682)
- Grenfell, J. L., Gebauer, S., Godolt, M., et al. 2013, *Astrobiology*, 13, 415, doi: [10.1089/ast.2012.0926](https://doi.org/10.1089/ast.2012.0926)
- Grimm, S. L., Demory, B.-O., Gillon, M., et al. 2018, *A&A*, 613, A68, doi: [10.1051/0004-6361/201732233](https://doi.org/10.1051/0004-6361/201732233)
- Gumsley, A. P., Chamberlain, K. R., Bleeker, W., et al. 2017, *Proceedings of the National Academy of Sciences*, 114, 1811
- Guzel-Seydim, Z. B., Greene, A. K., & Seydim, A. 2004, *LWT-Food Science and Technology*, 37, 453
- Haagen-Smit, A. J. 1952, *Industrial & Engineering Chemistry*, 44, 1342
- Hanelt, D., Melchersmann, B., Wiencke, C., & Nultsch, W. 1997, *Marine Ecology Progress Series*, 149, 255, doi: [10.3354/meps149255](https://doi.org/10.3354/meps149255)
- Harman, C. E., Felton, R., Hu, R., et al. 2018, *ApJ*, 866, 56, doi: [10.3847/1538-4357/aadd9b](https://doi.org/10.3847/1538-4357/aadd9b)
- Harman, C. E., Schwieterman, E. W., Schottelkotte, J. C., & Kasting, J. F. 2015, *ApJ*, 812, 137, doi: [10.1088/0004-637X/812/2/137](https://doi.org/10.1088/0004-637X/812/2/137)
- Helmig, D., Ganzeveld, L., Butler, T., & Oltmans, S. J. 2007, *Atmospheric Chemistry & Physics*, 7, 15, doi: [10.5194/acp-7-15-2007](https://doi.org/10.5194/acp-7-15-2007)
- Henshaw, T., & Laybourn-Parry, J. 2002, *Polar Biology*, 25, 744
- Hu, W., Liu, P., & Pei, H. 2003, *Chinese Science Bulletin*, 48, 862
- Hu, Y., & Yang, J. 2014, *Proceedings of the National Academy of Science*, 111, 629, doi: [10.1073/pnas.1315215111](https://doi.org/10.1073/pnas.1315215111)
- Huovinen, P., & Gómez, I. 2013, *Polar biology*, 36, 1319
- Iriti, M., & Faoro, F. 2007, *Water Air and Soil Pollution*, 187, 285, doi: [10.1007/s11270-007-9517-7](https://doi.org/10.1007/s11270-007-9517-7)
- Ji, A., Kasting, J. F., Cooke, G. J., Marsh, D. R., & Tsigaridis, K. 2023, *Royal Society Open Science*, 10, 230056, doi: [10.1098/rsos.230056](https://doi.org/10.1098/rsos.230056)
- Ji, A., Tomazzeli, O. G., Palancar, G. G., et al. 2024, *Journal of Geophysical Research: Atmospheres*, 129, e2023JD040610, doi: [10.1029/2023JD040610](https://doi.org/10.1029/2023JD040610)
- Jones, A. C., Gensemer, R. W., Stubblefield, W. A., et al. 2006, *Environmental Toxicology and Chemistry: An International Journal*, 25, 2683
- Joshi, M. M., Haberle, R. M., & Reynolds, R. T. 1997, *Icarus*, 129, 450, doi: [10.1006/icar.1997.5793](https://doi.org/10.1006/icar.1997.5793)
- Jung, P., Harion, F., Wu, S., et al. 2023, *Frontiers in Astronomy and Space Sciences*, 10, 5, doi: [10.3389/fspas.2023.1107371](https://doi.org/10.3389/fspas.2023.1107371)
- Kaltenegger, L., Lin, Z., & Rugheimer, S. 2020, *ApJ*, 904, 10, doi: [10.3847/1538-4357/abb9b2](https://doi.org/10.3847/1538-4357/abb9b2)

- Kaltenegger, L., & Sasselov, D. 2010, *ApJ*, 708, 1162, doi: [10.1088/0004-637X/708/2/1162](https://doi.org/10.1088/0004-637X/708/2/1162)
- Kappen, L. 1993, *Arctic*, 297
- Kasting, J. F., Whitmire, D. P., & Reynolds, R. T. 1993, *Icarus*, 101, 108, doi: [10.1006/icar.1993.1010](https://doi.org/10.1006/icar.1993.1010)
- Kim, J.-G., Yousef, A. E., & Dave, S. 1999, *Journal of food protection*, 62, 1071
- Kishimoto, N., & Arai, H. 2022, *Ozone: Science & Engineering*, 44, 265
- Klaunig, J. E., Kamendulis, L. M., & Hocevar, B. A. 2010, *Toxicologic pathology*, 38, 96
- Kleinböhl, A., Willacy, K., Friedson, A. J., Chen, P., & Swain, M. R. 2018, *ApJ*, 862, 92, doi: [10.3847/1538-4357/aaca36](https://doi.org/10.3847/1538-4357/aaca36)
- Kopparapu, R., Arney, G., Haqq-Misra, J., Lustig-Yaeger, J., & Villanueva, G. 2021, *ApJ*, 908, 164, doi: [10.3847/1538-4357/abd7f7](https://doi.org/10.3847/1538-4357/abd7f7)
- Kozakis, T., & Kaltenegger, L. 2020, *AJ*, 160, 225, doi: [10.3847/1538-3881/abb9ac](https://doi.org/10.3847/1538-3881/abb9ac)
- Kozakis, T., Kaltenegger, L., & Hoard, D. W. 2018, *ApJ*, 862, 69, doi: [10.3847/1538-4357/aacbc7](https://doi.org/10.3847/1538-4357/aacbc7)
- Kozakis, T., Mendonça, J. M., & Buchhave, L. A. 2022, *A&A*, 665, A156, doi: [10.1051/0004-6361/202244164](https://doi.org/10.1051/0004-6361/202244164)
- Large, R. R., Mukherjee, I., Gregory, D., et al. 2019, *Mineralium Deposita*, 54, 485, doi: [10.1007/s00126-019-00873-9](https://doi.org/10.1007/s00126-019-00873-9)
- Leger, A., Pirre, M., & Marceau, F. J. 1993, *A&A*, 277, 309
- Lehmer, O. R., Catling, D. C., Parenteau, M. N., & Hoehler, T. M. 2018, *ApJ*, 859, 171, doi: [10.3847/1538-4357/aac104](https://doi.org/10.3847/1538-4357/aac104)
- Lewis, N. T., Lambert, F. H., Boutle, I. A., et al. 2018, *ApJ*, 854, 171, doi: [10.3847/1538-4357/aaad0a](https://doi.org/10.3847/1538-4357/aaad0a)
- Lin, Z., MacDonald, R. J., Kaltenegger, L., & Wilson, D. J. 2021, *MNRAS*, 505, 3562, doi: [10.1093/mnras/stab1486](https://doi.org/10.1093/mnras/stab1486)
- Lingam, M., & Loeb, A. 2019, *MNRAS*, 485, 5924, doi: [10.1093/mnras/stz847](https://doi.org/10.1093/mnras/stz847)
- Loose, B., Miller, L. A., Elliott, S., & Papakyriakou, T. 2011, *Oceanography*, 24, 202
- Loose, B., Schlosser, P., Perovich, D., et al. 2011, *Tellus Series B Chemical and Physical Meteorology B*, 63, 23, doi: [10.1111/j.1600-0889.2010.00506.x](https://doi.org/10.1111/j.1600-0889.2010.00506.x)
- Loyd, R. O. P., France, K., Youngblood, A., et al. 2016, *ApJ*, 824, 102, doi: [10.3847/0004-637X/824/2/102](https://doi.org/10.3847/0004-637X/824/2/102)
- Luger, R., & Barnes, R. 2015, in *American Astronomical Society Meeting Abstracts*, Vol. 225, American Astronomical Society Meeting Abstracts #225, 407.04
- Lushchak, V. I. 2011, *Aquatic toxicology*, 101, 13
- Lykkesfeldt, J., & Svendsen, O. 2007, *The veterinary journal*, 173, 502
- Lyons, T. W., Diamond, C. W., Planavsky, N. J., Reinhard, C. T., & Li, C. 2021, *Astrobiology*, 21, 906, doi: [10.1089/ast.2020.2418](https://doi.org/10.1089/ast.2020.2418)
- Lyons, T. W., Reinhard, C. T., & Planavsky, N. J. 2014, *Nature*, 506, 307, doi: [10.1038/nature13068](https://doi.org/10.1038/nature13068)
- Macdonald, E., Paradise, A., Menou, K., & Lee, C. 2022, *MNRAS*, 513, 2761, doi: [10.1093/mnras/stac1040](https://doi.org/10.1093/mnras/stac1040)
- Madhusudhan, N., Piette, A. A. A., & Constantinou, S. 2021, *ApJ*, 918, 1, doi: [10.3847/1538-4357/abfd9c](https://doi.org/10.3847/1538-4357/abfd9c)
- Malashock, D. A., Delang, M. N., Becker, J. S., et al. 2022, *The Lancet Planetary Health*, 6, e958
- Malashock, D. A., DeLang, M. N., Becker, J. S., et al. 2022, *Environmental Research Letters*, 17, 054023, doi: [10.1088/1748-9326/ac66f3](https://doi.org/10.1088/1748-9326/ac66f3)
- Marcos-Arenal, P., Cerdán, L., Burillo-Villalobos, M., et al. 2022, *Universe*, 8, 624, doi: [10.3390/universe8120624](https://doi.org/10.3390/universe8120624)
- McMinn, A., Ryan, K., Ralph, P., & Pankowski, A. 2007, *Marine Biology*, 151, 985
- McNaught, A. D., Wilkinson, A., et al. 1997, *Compendium of chemical terminology*, Vol. 1669 (Blackwell Science Oxford)
- Meadows, V. S., Arney, G. N., Schwieterman, E. W., et al. 2018, *Astrobiology*, 18, 133, doi: [10.1089/ast.2016.1589](https://doi.org/10.1089/ast.2016.1589)
- Méndez, A., Rivera-Valentín, E. G., Schulze-Makuch, D., et al. 2021, *Astrobiology*, 21, 1017, doi: [10.1089/ast.2020.2342](https://doi.org/10.1089/ast.2020.2342)
- Menzel, D. B. 1984, *Journal of Toxicology and Environmental Health*
- Najafi, M. B. H., & Khodaparast, M. H. 2009, *Food control*, 20, 27
- Norris, J., & Olsen, J. 1991, *Phycologia*, 30, 315
- Nuvolone, D., Petri, D., & Voller, F. 2018, *Environmental Science and Pollution Research*, 25, 8074
- Olson, S., Jansen, M. F., Abbot, D. S., Halevy, I., & Goldblatt, C. 2022, *Geophys. Res. Lett.*, 49, e95748, doi: [10.1029/2021GL095748](https://doi.org/10.1029/2021GL095748)
- Otegi, J. F., Bouchy, F., & Helled, R. 2020, *A&A*, 634, A43, doi: [10.1051/0004-6361/201936482](https://doi.org/10.1051/0004-6361/201936482)
- Peacock, S. 2020, *Habitable Zones and M dwarf Activity across Time ("HAZMAT")*, Version 1, STScI/MAST, doi: [10.17909/T9-J6BZ-5G89](https://doi.org/10.17909/T9-J6BZ-5G89)
- Peacock, S., Barman, T., Shkolnik, E. L., Hauschildt, P. H., & Baron, E. 2019, *ApJ*, 871, 235, doi: [10.3847/1538-4357/aaf891](https://doi.org/10.3847/1538-4357/aaf891)
- Pidhorodetska, D., Fauchez, T. J., Villanueva, G. L., Domagal-Goldman, S. D., & Kopparapu, R. K. 2020, *ApJL*, 898, L33, doi: [10.3847/2041-8213/aba4a1](https://doi.org/10.3847/2041-8213/aba4a1)
- Pierrehumbert, R. T., & Hammond, M. 2019, *Annual Review of Fluid Mechanics*, 51, 275, doi: [10.1146/annurev-fluid-010518-040516](https://doi.org/10.1146/annurev-fluid-010518-040516)

- Pineda, J. S., Youngblood, A., & France, K. 2021, *ApJ*, 918, 40, doi: [10.3847/1538-4357/ac0aea](https://doi.org/10.3847/1538-4357/ac0aea)
- Poulton, S. W., Bekker, A., Cumming, V. M., et al. 2021, *Nature*, 592, 232
- Premjit, Y., Sruthi, N., Pandiselvam, R., & Kothakota, A. 2022, *Comprehensive Reviews in Food Science and Food Safety*, 21, 1054
- Pritchard, D. W., Hurd, C. L., Beardall, J., & Hepburn, C. D. 2013, *Journal of Phycology*, 49, 867
- Proedrou, E., & Hocke, K. 2016, *Earth, Planets and Space*, 68, 96, doi: [10.1186/s40623-016-0461-x](https://doi.org/10.1186/s40623-016-0461-x)
- Rajpurohit, A. S., Reylé, C., Allard, F., et al. 2013, *A&A*, 556, A15, doi: [10.1051/0004-6361/201321346](https://doi.org/10.1051/0004-6361/201321346)
- Ramirez, R. M. 2020, *Scientific Reports*, 10, 7432, doi: [10.1038/s41598-020-64436-z](https://doi.org/10.1038/s41598-020-64436-z)
- Ramus, J., Beale, S., & Mauzerall, D. 1976, *Marine Biology*, 37, 231
- Ramya, A., Dhevagi, P., Poornima, R., et al. 2023, *Environmental Research*, 236, 116816, doi: [10.1016/j.envres.2023.116816](https://doi.org/10.1016/j.envres.2023.116816)
- Rao, M. V., & Davis, K. R. 2001, *Planta*, 213, 682
- Reinhard, C. T., Olson, S. L., Schwieterman, E. W., & Lyons, T. W. 2017, *Astrobiology*, 17, 287, doi: [10.1089/ast.2016.1598](https://doi.org/10.1089/ast.2016.1598)
- Renaud, J. P., Henning, W. G., Saxena, P., et al. 2021, *PSJ*, 2, 4, doi: [10.3847/PSJ/abc0f3](https://doi.org/10.3847/PSJ/abc0f3)
- Ribas, I., Bolmont, E., Selsis, F., et al. 2016, *A&A*, 596, A111, doi: [10.1051/0004-6361/201629576](https://doi.org/10.1051/0004-6361/201629576)
- Rich, S. 1964, *Annual Review of Phytopathology*, 2, 253
- Ridgway, R. J., Zamyatina, M., Mayne, N. J., et al. 2023, *MNRAS*, 518, 2472, doi: [10.1093/mnras/stac3105](https://doi.org/10.1093/mnras/stac3105)
- Rojas-Valencia, M. 2011, *Virus*, 3, 263
- Rugheimer, S., & Kaltenecker, L. 2018, *ApJ*, 854, 19, doi: [10.3847/1538-4357/aaa47a](https://doi.org/10.3847/1538-4357/aaa47a)
- Rugheimer, S., Kaltenecker, L., Segura, A., Linsky, J., & Mohanty, S. 2015, *ApJ*, 809, 57, doi: [10.1088/0004-637X/809/1/57](https://doi.org/10.1088/0004-637X/809/1/57)
- Safonova, M., Mathur, A., Basak, S., Bora, K., & Agrawal, S. 2021, *European Physical Journal Special Topics*, 230, 2207, doi: [10.1140/epjs/s11734-021-00211-z](https://doi.org/10.1140/epjs/s11734-021-00211-z)
- Salazar, A. M., Olson, S. L., Komacek, T. D., Stephens, H., & Abbot, D. S. 2020, *ApJL*, 896, L16, doi: [10.3847/2041-8213/ab94c1](https://doi.org/10.3847/2041-8213/ab94c1)
- Sandermann Jr, H. 1996, *Annual review of phytopathology*, 34, 347
- Sandu, A., Verwer, J., Blom, J., et al. 1997, *Atmospheric environment*, 31, 3459
- Scheucher, M., Herbst, K., Schmidt, V., et al. 2020, *ApJ*, 893, 12, doi: [10.3847/1538-4357/ab7b74](https://doi.org/10.3847/1538-4357/ab7b74)
- Schwieterman, E. W., Reinhard, C. T., Olson, S. L., Harman, C. E., & Lyons, T. W. 2019, *ApJ*, 878, 19, doi: [10.3847/1538-4357/ab1d52](https://doi.org/10.3847/1538-4357/ab1d52)
- Schwieterman, E. W., Meadows, V. S., Domagal-Goldman, S. D., et al. 2016, *ApJL*, 819, L13, doi: [10.3847/2041-8205/819/1/L13](https://doi.org/10.3847/2041-8205/819/1/L13)
- Schwieterman, E. W., Kiang, N. Y., Parenteau, M. N., et al. 2018, *Astrobiology*, 18, 663, doi: [10.1089/ast.2017.1729](https://doi.org/10.1089/ast.2017.1729)
- Segura, A., Meadows, V. S., Kasting, J. F., Crisp, D., & Cohen, M. 2007, *A&A*, 472, 665, doi: [10.1051/0004-6361:200666663](https://doi.org/10.1051/0004-6361:200666663)
- Segura, A., Walkowicz, L. M., Meadows, V., Kasting, J., & Hawley, S. 2010, *Astrobiology*, 10, 751, doi: [10.1089/ast.2009.0376](https://doi.org/10.1089/ast.2009.0376)
- Sergeev, D. E., Mayne, N. J., Bendall, T., et al. 2023, *Geoscientific Model Development*, 16, 5601, doi: [10.5194/gmd-16-5601-2023](https://doi.org/10.5194/gmd-16-5601-2023)
- Sharkey, T. D., Wiberley, A. E., & Donohue, A. R. 2008, *Annals of botany*, 101, 5
- Showman, A. P., & Polvani, L. M. 2011, *ApJ*, 738, 71, doi: [10.1088/0004-637X/738/1/71](https://doi.org/10.1088/0004-637X/738/1/71)
- Sies, H., Berndt, C., & Jones, D. P. 2017, *Annual review of biochemistry*, 86, 715
- Sillman, S. 1999, *Atmospheric Environment*, 33, 1821
- Silva, R. A., West, J. J., Zhang, Y., et al. 2013, *Environmental Research Letters*, 8, 034005
- Squire, O. J., Archibald, A. T., Abraham, N. L., et al. 2014, *Atmospheric Chemistry & Physics*, 14, 1011, doi: [10.5194/acp-14-1011-2014](https://doi.org/10.5194/acp-14-1011-2014)
- Steadman, J. A., Large, R. R., Blamey, N. J., et al. 2020, *Precambrian Research*, 343, 105722, doi: [10.1016/j.precamres.2020.105722](https://doi.org/10.1016/j.precamres.2020.105722)
- Stokinger, H. 1965, *Archives of Environmental Health: An International Journal*, 10, 719
- Sun, H. Z., Yu, P., Lan, C., et al. 2022, *The Innovation*, 3, 100246, doi: [10.1016/j.xinn.2022.100246](https://doi.org/10.1016/j.xinn.2022.100246)
- Suzuki, Y., Kudoh, S., & Takahashi, M. 1997, *Journal of Marine Systems*, 11, 111, doi: [10.1016/S0924-7963\(96\)00032-2](https://doi.org/10.1016/S0924-7963(96)00032-2)
- Tabataba-Vakili, F., Grenfell, J. L., Griebmeier, J. M., & Rauer, H. 2016, *A&A*, 585, A96, doi: [10.1051/0004-6361/201425602](https://doi.org/10.1051/0004-6361/201425602)
- Tian, F., France, K., Linsky, J. L., Mauas, P. J. D., & Vieytes, M. C. 2014, *Earth and Planetary Science Letters*, 385, 22, doi: [10.1016/j.epsl.2013.10.024](https://doi.org/10.1016/j.epsl.2013.10.024)
- Tilley, M. A., Segura, A., Meadows, V., Hawley, S., & Davenport, J. 2019, *Astrobiology*, 19, 64, doi: [10.1089/ast.2017.1794](https://doi.org/10.1089/ast.2017.1794)
- Tjoa, J. N. K. Y., Mueller, M., & van der Tak, F. F. S. 2020, *A&A*, 636, A50, doi: [10.1051/0004-6361/201937035](https://doi.org/10.1051/0004-6361/201937035)

- Truitt, A. R., Young, P. A., Walker, S. I., & Spacek, A. 2020, *AJ*, 159, 55, doi: [10.3847/1538-3881/ab4e93](https://doi.org/10.3847/1538-3881/ab4e93)
- Turbet, M., Fauchez, T. J., Sergeev, D. E., et al. 2022, *PSJ*, 3, 211, doi: [10.3847/PSJ/ac6cf0](https://doi.org/10.3847/PSJ/ac6cf0)
- Turner, M. C., Jerrett, M., Pope III, C. A., et al. 2016, *American journal of respiratory and critical care medicine*, 193, 1134
- Val Martin, M., Heald, C. L., & Arnold, S. R. 2014, *Geophys. Res. Lett.*, 41, 2988, doi: [10.1002/2014GL059651](https://doi.org/10.1002/2014GL059651)
- Valavanidis, A., Vlachogianni, T., Fiotakis, K., & Loridas, S. 2013, *International journal of environmental research and public health*, 10, 3886
- Way, M. J., Aleinov, I., Amundsen, D. S., et al. 2017, *ApJS*, 231, 12, doi: [10.3847/1538-4365/aa7a06](https://doi.org/10.3847/1538-4365/aa7a06)
- Wert, E. C., Lew, J., & Rakness, K. L. 2017, *Journal-American Water Works Association*, 109, E302
- Wesely, M. L. 1989, *Atmospheric Environment*, 23, 1293, doi: [10.1016/0004-6981\(89\)90153-4](https://doi.org/10.1016/0004-6981(89)90153-4)
- Wesely, M. L., & Hicks, B. B. 2000, *Atmospheric Environment*, 34, 2261, doi: [10.1016/S1352-2310\(99\)00467-7](https://doi.org/10.1016/S1352-2310(99)00467-7)
- Wilson, D. J., Froning, C., Duvvuri, G., et al. 2021a, *Mega-MUSCLES Semi-empirical SED of TRAPPIST-1, Version 1*, Zenodo. <https://doi.org/10.5281/zenodo.4556130>
- Wilson, D. J., Froning, C. S., Duvvuri, G. M., et al. 2021b, *ApJ*, 911, 18, doi: [10.3847/1538-4357/abe771](https://doi.org/10.3847/1538-4357/abe771)
- Wordsworth, R., & Pierrehumbert, R. 2014, *ApJL*, 785, L20, doi: [10.1088/2041-8205/785/2/L20](https://doi.org/10.1088/2041-8205/785/2/L20)
- World Health Organization, et al. 2000, *Air quality guidelines for Europe* (World Health Organization. Regional Office for Europe)
- Yassin Jaziri, A., Charnay, B., Selsis, F., Leconte, J., & Lefèvre, F. 2022, *Climate of the Past*, 18, 2421, doi: [10.5194/cp-18-2421-2022](https://doi.org/10.5194/cp-18-2421-2022)
- Yates, J. S., Palmer, P. I., Manners, J., et al. 2020, *MNRAS*, 492, 1691, doi: [10.1093/mnras/stz3520](https://doi.org/10.1093/mnras/stz3520)
- Youngblood, A., France, K., Loyd, R. O. P., et al. 2016, *ApJ*, 824, 101, doi: [10.3847/0004-637X/824/2/101](https://doi.org/10.3847/0004-637X/824/2/101)
- Zahnle, K. J., Catling, D. C., & Claire, M. W. 2013, *Chemical Geology*, 362, 26, doi: [10.1016/j.chemgeo.2013.08.004](https://doi.org/10.1016/j.chemgeo.2013.08.004)
- Zhao, Z., Liu, Y., Li, W., Liu, H., & Man, K. 2021, *ApJL*, 910, L8, doi: [10.3847/2041-8213/abebe6](https://doi.org/10.3847/2041-8213/abebe6)
- Zhen, S., van Iersel, M. W., & Bugbee, B. 2022, *New Phytologist*, 236, 538
- Zieba, S., Kreidberg, L., Ducrot, E., et al. 2023, *arXiv e-prints*, arXiv:2306.10150, doi: [10.48550/arXiv.2306.10150](https://doi.org/10.48550/arXiv.2306.10150)